A comprehensive kinetic model for Dimethyl ether and Dimethoxymethane oxidation and NOx interaction utilizing experimental laminar flame speed measurements at elevated pressure and temperature

Krishna Prasad Shrestha[1], Sven Eckart[2], Ayman M. Elbaz [3], Binod Raj Giri[3], Chris Fritsche[2], Lars Seidel*[4], William L. Roberts[3], Hartmut Krause[2], Fabian Mauss[1]

1. Thermodynamics and Thermal Process Engineering, Brandenburg University of Technology, Siemens-Halske Ring 8, 03046 Cottbus, Germany
2. Chair of Gas and Heat Technology, Technische Universität Bergakademie Freiberg, Gustav-Zeuner-Straße 7, Freiberg, Germany
3. Clean Combustion Research Center, King Abdullah University of Science and Technology, Thuwal 23955-6900, Saudi Arabia
4. LOGE Deutschland GmbH, Burger Chaussee 25, 03044 Cottbus, Germany

***Corresponding author:**

E-mail: Lars.Seidel@logesoft.com

Krishna Prasad Shrestha, e-mail: shrestha@b-tu.de

Combustion and Flame 2020, doi: 10.1016/j.combustflame.2020.04.016

https://doi.org/10.1016/j.combustflame.2020.04.016

Supplementary Material

1. Laminar flame speed

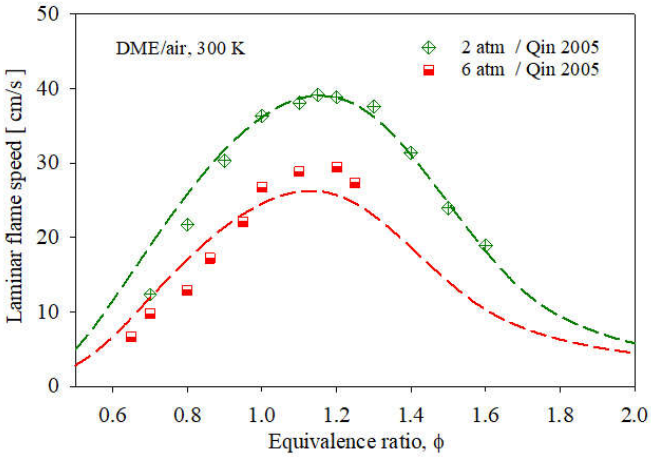

Figure S1: Laminar flame speed of DME/air at 2 and 6 atm. Symbols experimental data from [1]; lines: this work.

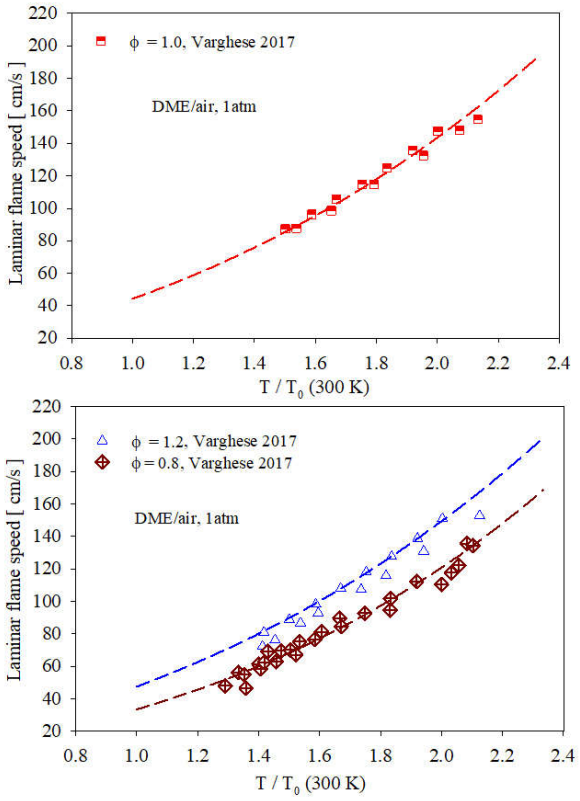

Figure S2: Laminar flame speed of DME/air at as a function of temperature at ϕ = 1.0 (top), 0.8 and 1.2 (bottom). Symbols experimental data from [2]; lines: this work.

2. Jet stirred reactor

2.1 DME reaction flow and sensitivity analysis for condition shown in Figure 8 at 600 K

To explore the important reactions for DME degradation at 600 K for the condition shown in Figure 8 reaction flow analysis and sensitivity analysis is performed. Figure S3 shows the integrated mass flux based on C-atoms (only major paths are shown) and Figure S4 shows the reaction sensitivity analysis. In Figure S3 percentage in the arrow means that the species is consumed at that amount (in total) to form another species. The major consumptions paths are only shown.

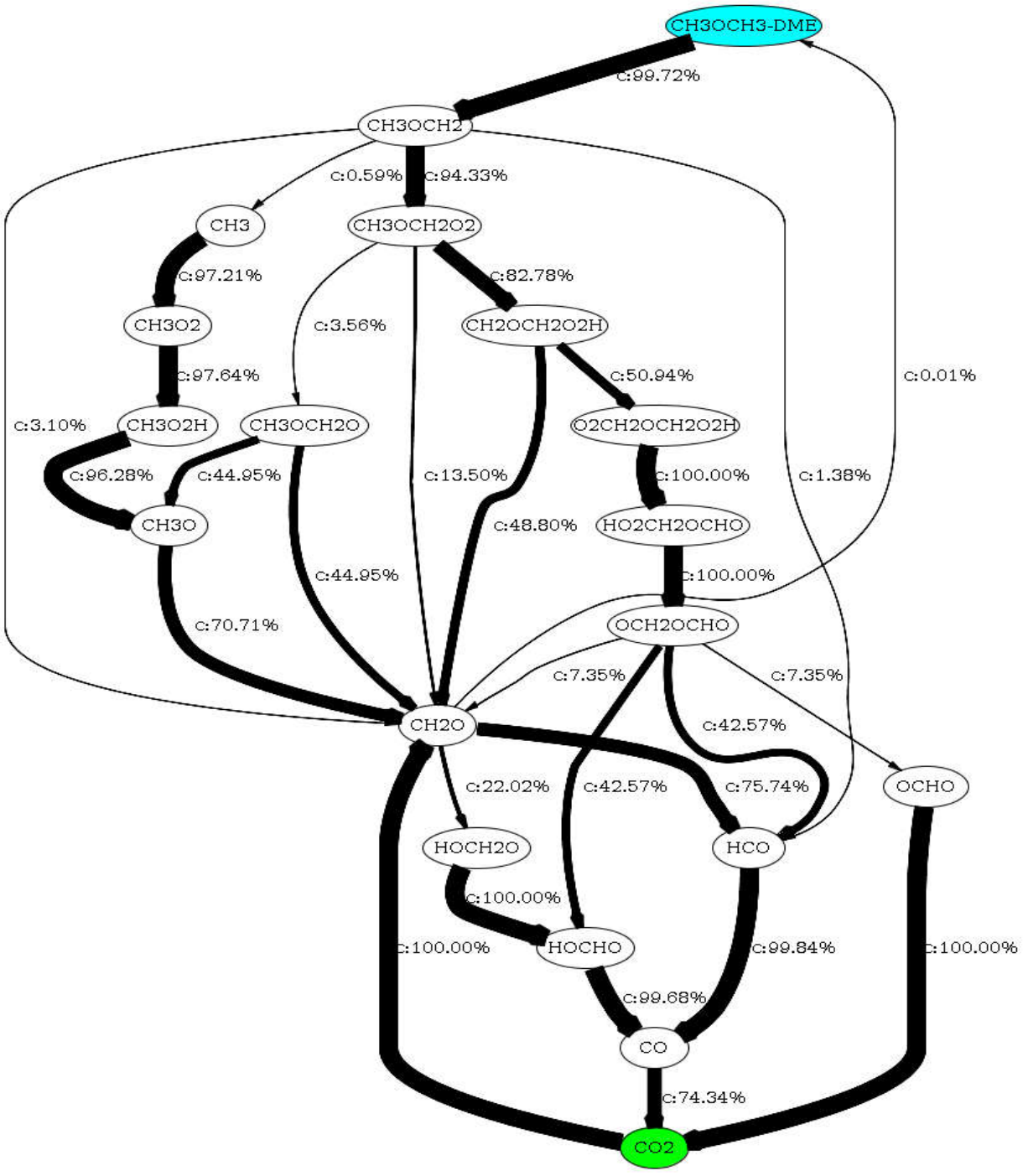

Figure S3: Reaction flow analysis based on C-atom during oxidation of DME(CH_3OCH_3)/O_2/N_2 at ϕ = 1.0, 10 atm, and τ = 1.0 s in a jet-stirred reactor for the condition shown in Figure 8 at 600 K.

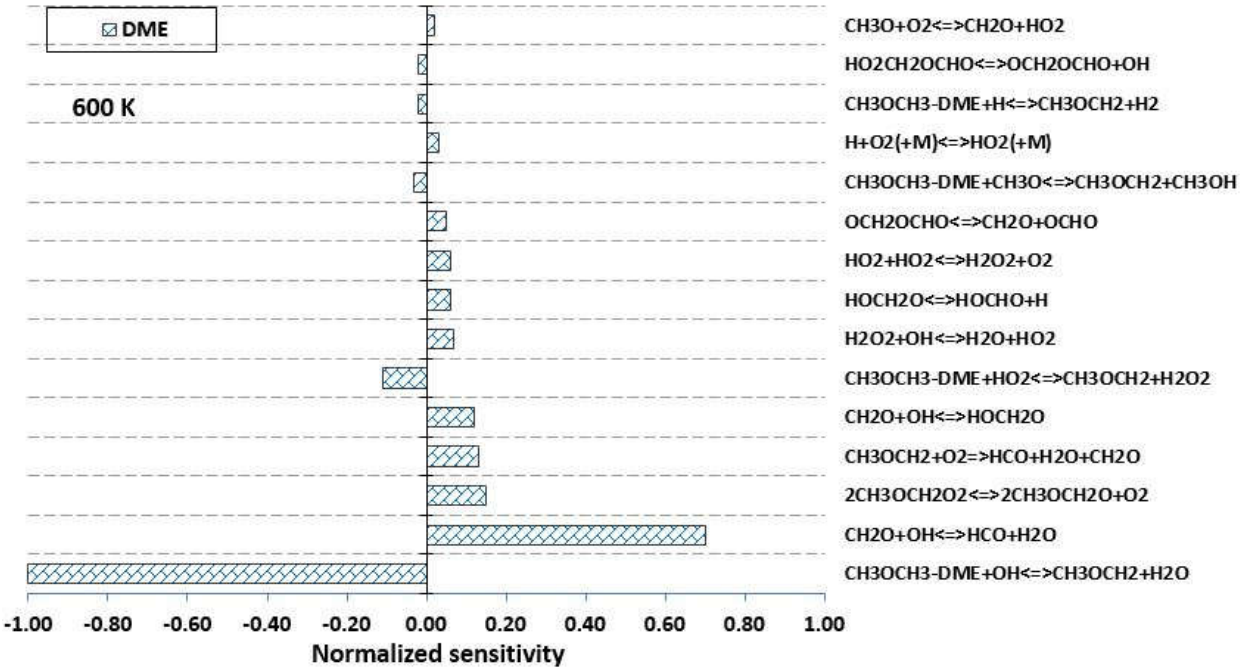

Figure S4: Normalized reaction sensitivity at 600 K during DME/O_2/N_2 oxidation at 10 atm for the condition shown in Figure 8 towards DME.

2.2 DMM reaction flow and sensitivity analysis for condition shown in Figure 11 at 600 K

To investigate the reaction paths and important reactions at low temperature during DMM oxidation, reaction flow and sensitivity analysis at 600 K is also performed (for the condition of Figure 11 which are shown in Figure S5 and Figure S6. At this temperature, DMM can undergo H-atom abstraction not only by OH and HO_2 but also by CH_3O_2 radical to form R1 (46%) and R2 (50%). Unlike at 900 K (Figure 13), the reaction DMM + OH (see Fig. S6) exhibits the highest sensitivity at this temperature (600 K). Further, R1 radicals exclusively (99%) undergoes O_2 addition path which is contrary to 900 K case where thermal dissociation is favored. In the case of radical R2, it does not undergo the O_2 addition channel and prefers the same thermal dissociation channel (R2=$CH_3OCHO+CH_3$). This explains why DMM is not exhibiting a marked NTC region

as found for DME (see Figure 8 and section 5.5.1). Additional illustrations for the model validation of DMM in a JSR are provided in Fig. S12 – Fig. S14.

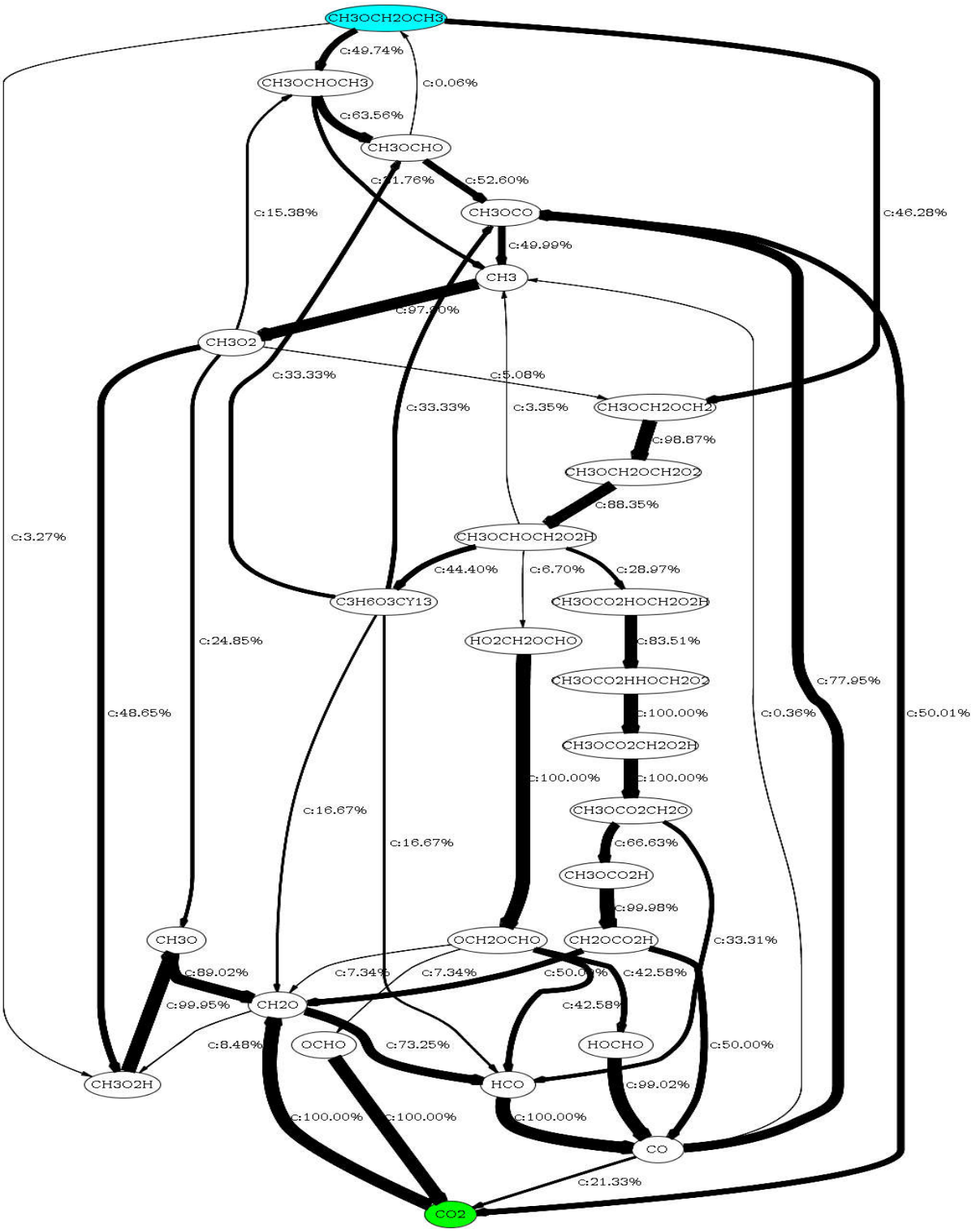

Figure S5: Reaction flow analysis based on C-atom during oxidation of DMM/O_2/N_2 in a jet-stirred reactor for the condition shown in Figure 11 at 600 K.

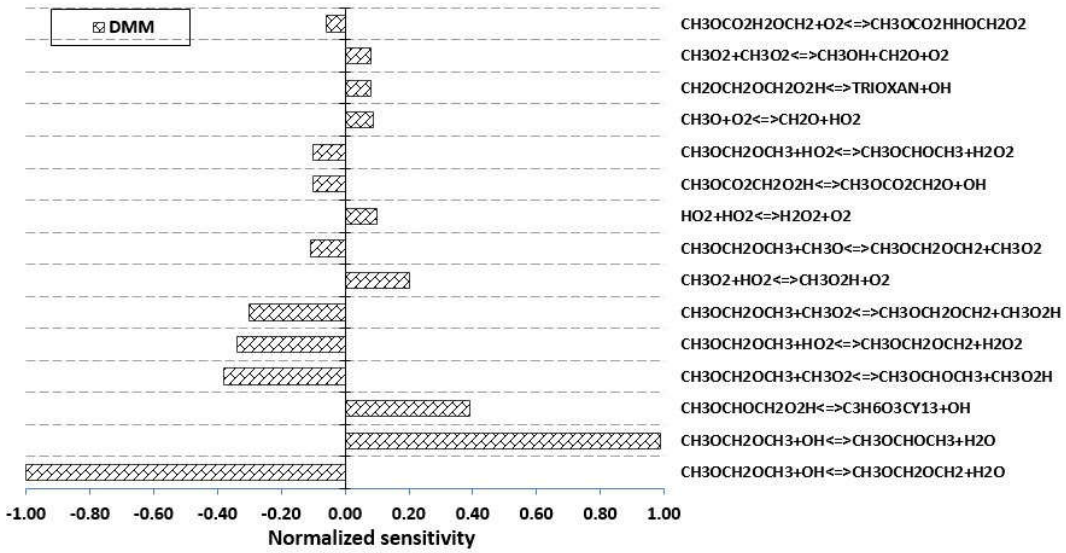

Figure S6: Normalized reaction sensitivity at 600 K during DMM/O_2/N_2 oxidation at 10 atm for the condition shown in Figure 11 towards DMM.

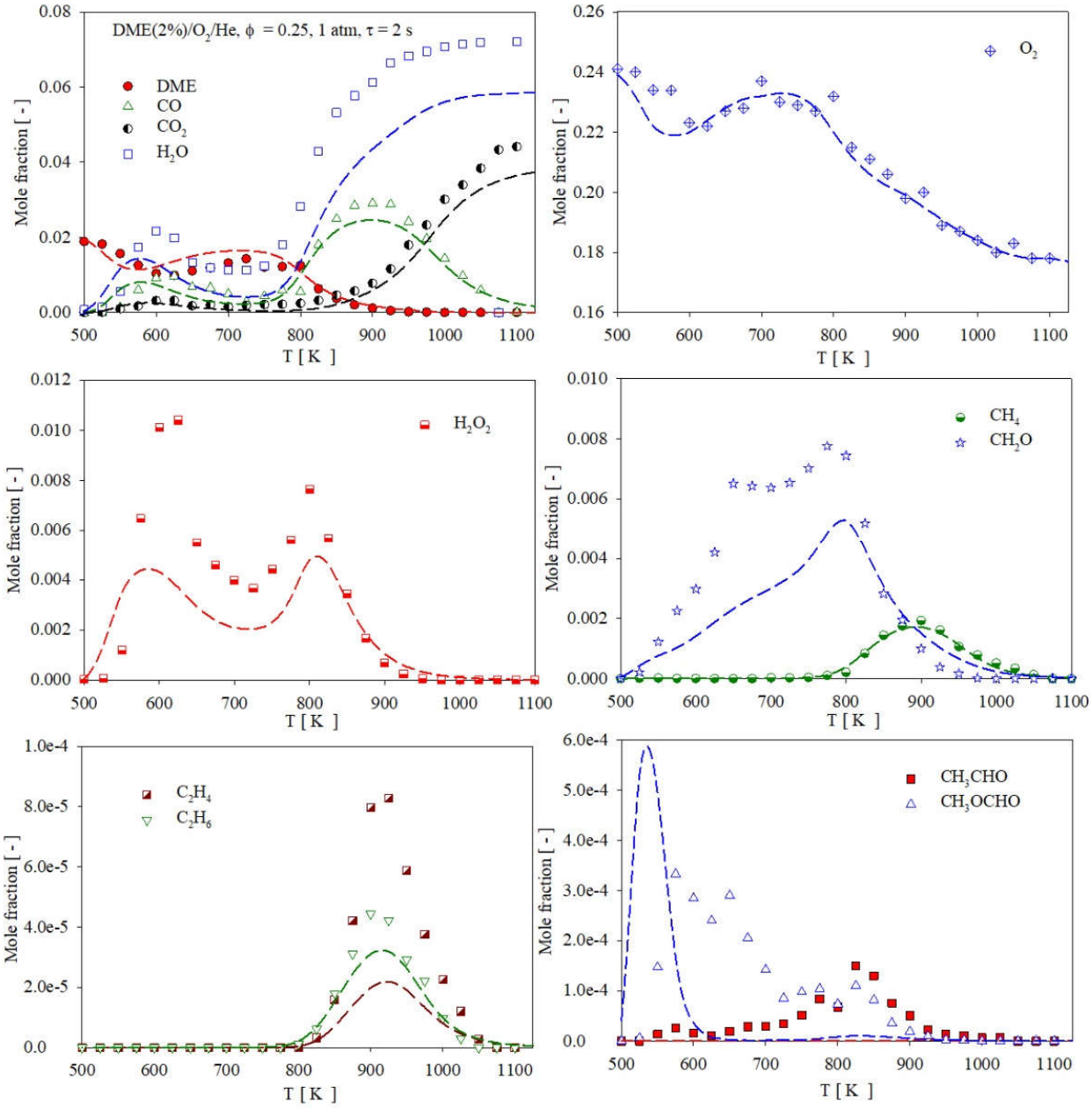

Figure S7: Oxidation of DME/O_2/He in a jet-stirred reactor at 1 atm and ϕ = 0.25. Symbols: experimental data from Rodriguez et al. [3]; lines: this work.

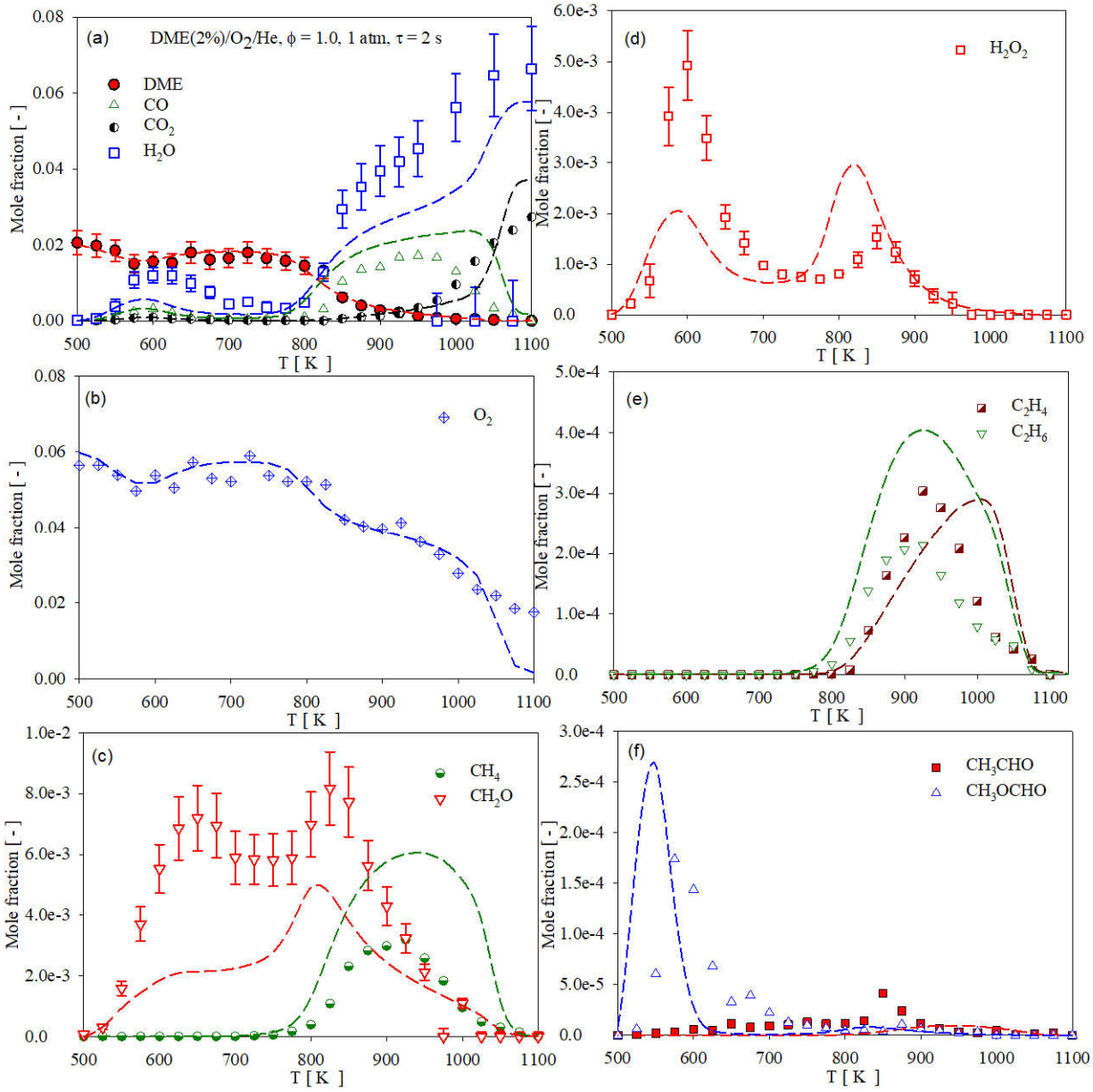

Figure S8: Oxidation of DME/O_2/He in a jet-stirred reactor at 1 atm and ϕ = 1. Symbols: experimental data from Rodriguez et al. [3]; lines: this work.

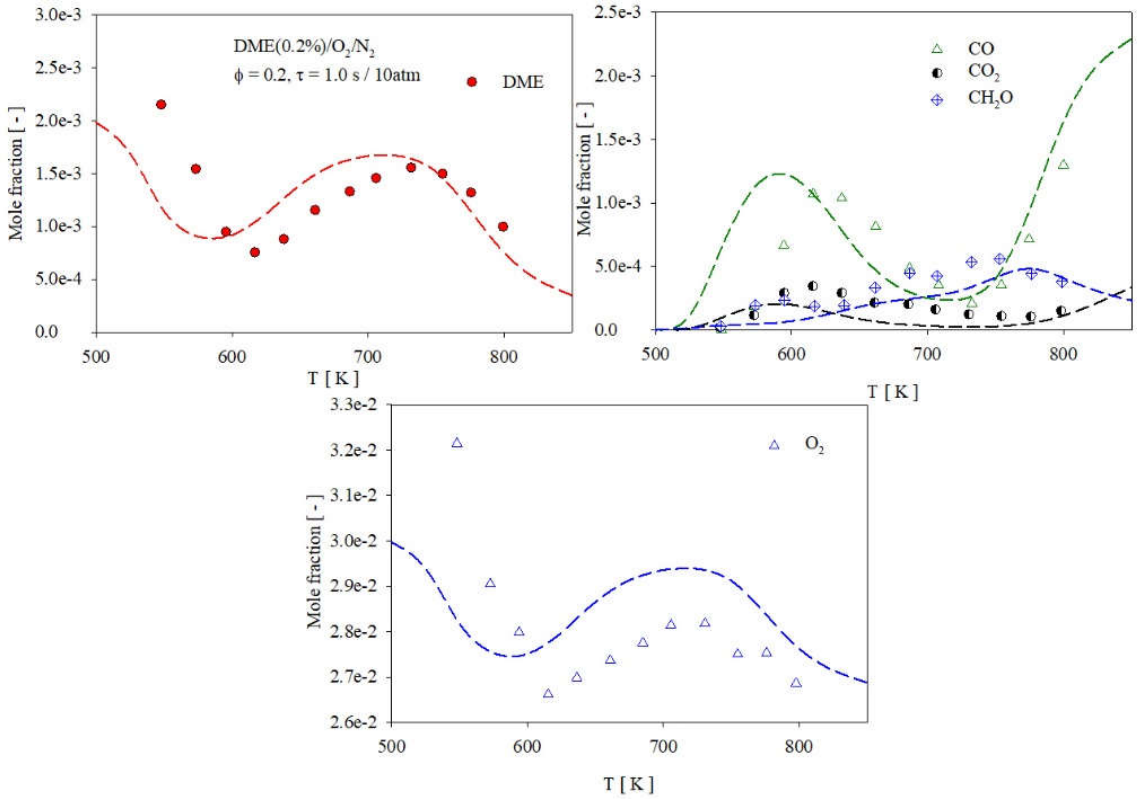

Figure S9: Oxidation of DME(0.1%)/O_2/N_2 in a jet-stirred reactor at 10 atm and ϕ = 0.2. Symbols: experimental data from Dagaut et al. [4]; lines: this work.

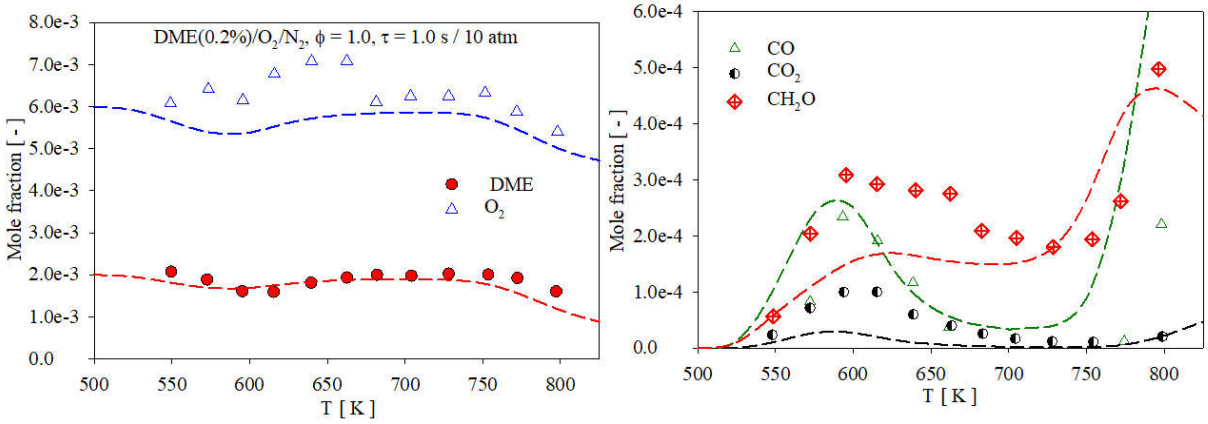

Figure S10: Oxidation of DME(0.2%)/O_2/N_2 in a jet-stirred reactor at 10 atm and ϕ = 1.0. Symbols: experimental data from Dagaut et al. [4]; lines: this work.

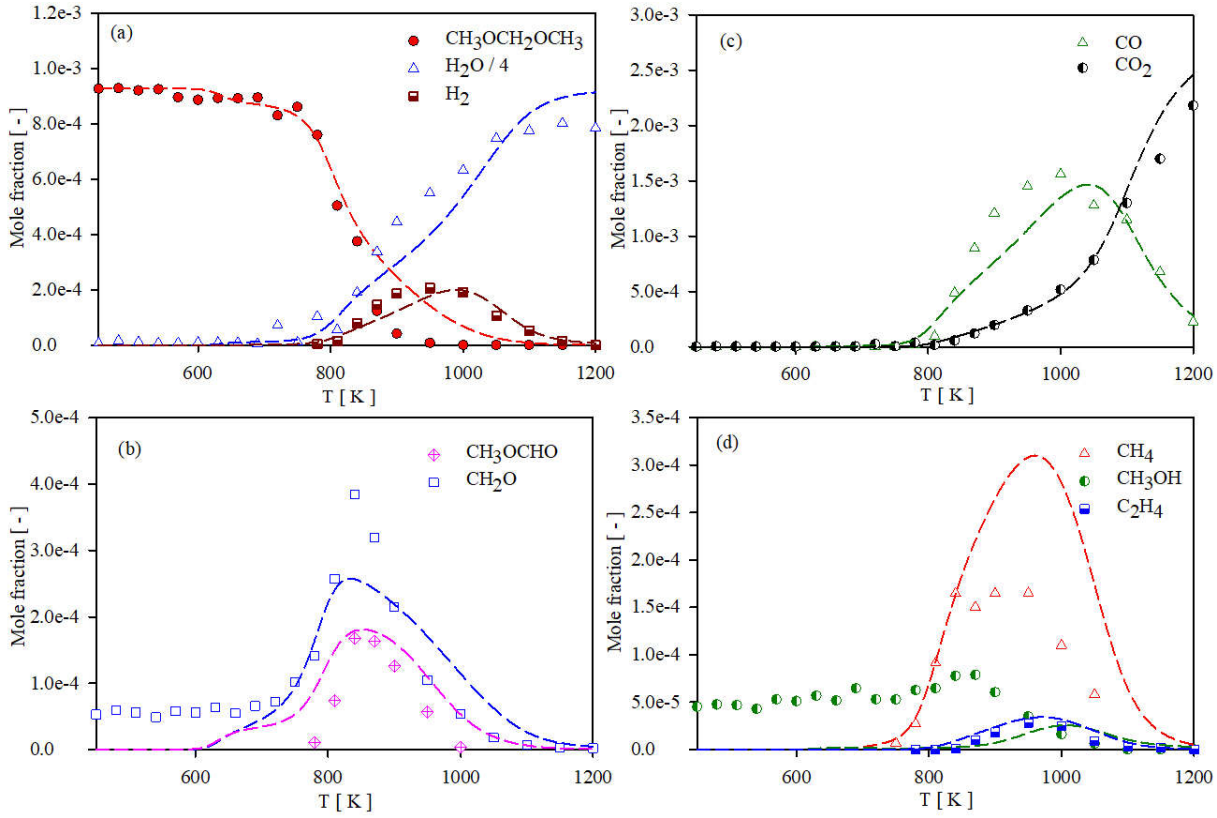

Figure S11: oxidation of DMM($CH_3OCH_2OCH_3$)/O_2/N_2 at ϕ = 0.5, 10 atm, and τ = 0.7 s in a jet-stirred reactor. Symbols: experimental data from Sun et al. [5], Lines: this model.

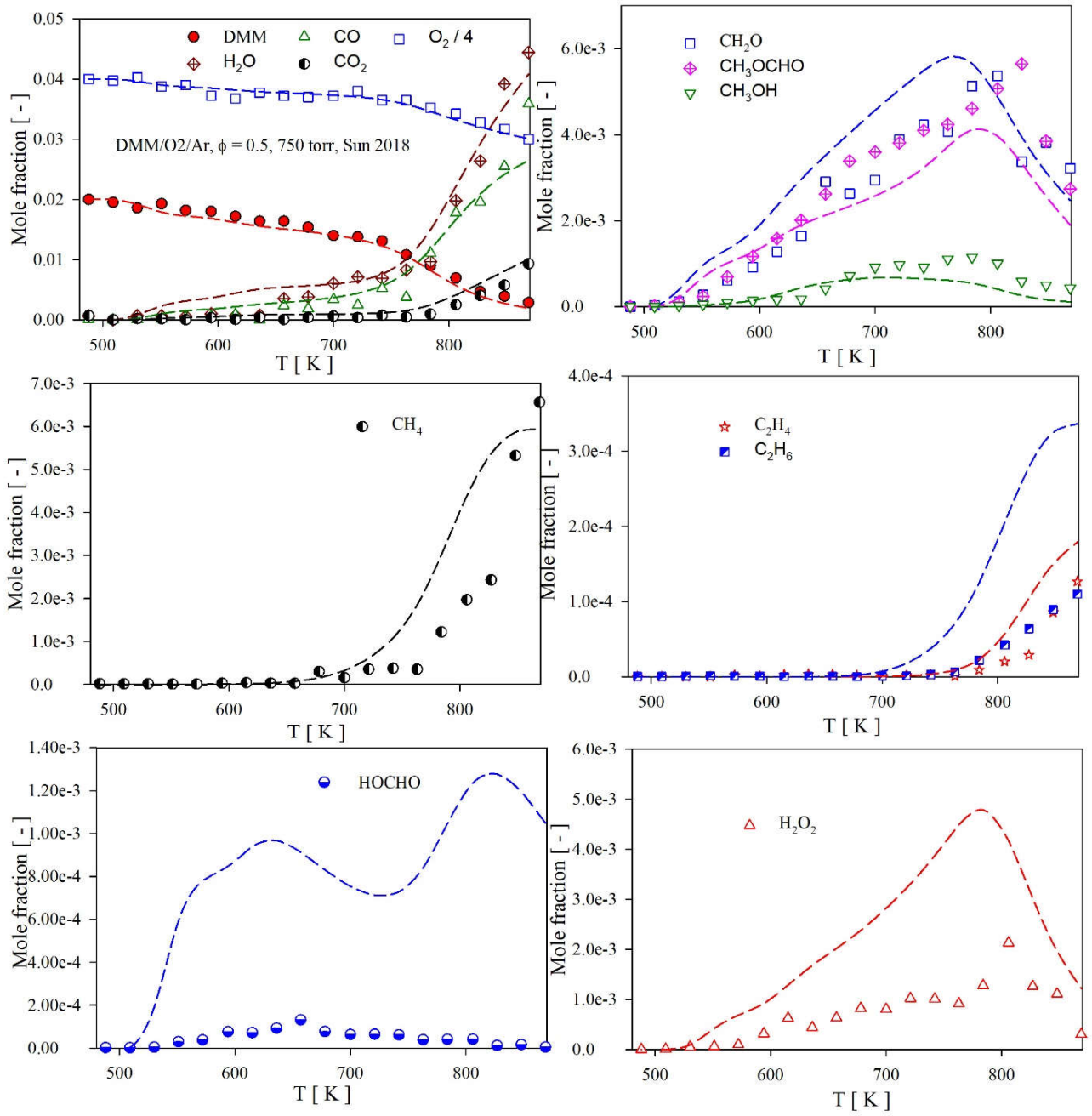

Figure S12: Oxidation of DMM/O_2/Ar in a jet-stirred reactor at 750 torr and ϕ = 0.5. Symbols: experimental data from Sun et al. [5]; lines: this work.

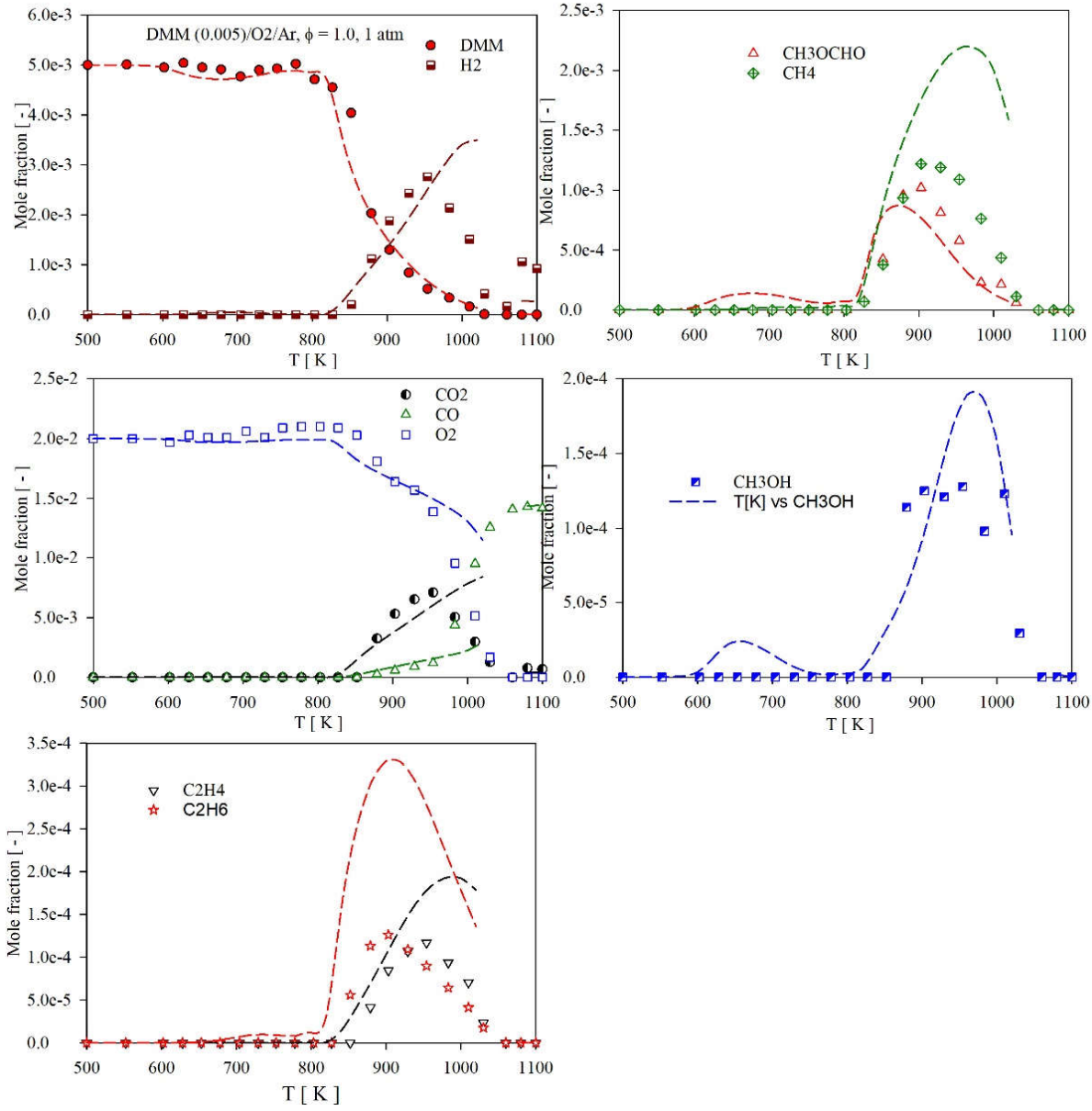

Figure S13: Oxidation of DMM/O_2/Ar in a jet-stirred reactor at 1 atm and ϕ = 1.0. Symbols: experimental data from Gao et al. [6]; lines: this work.

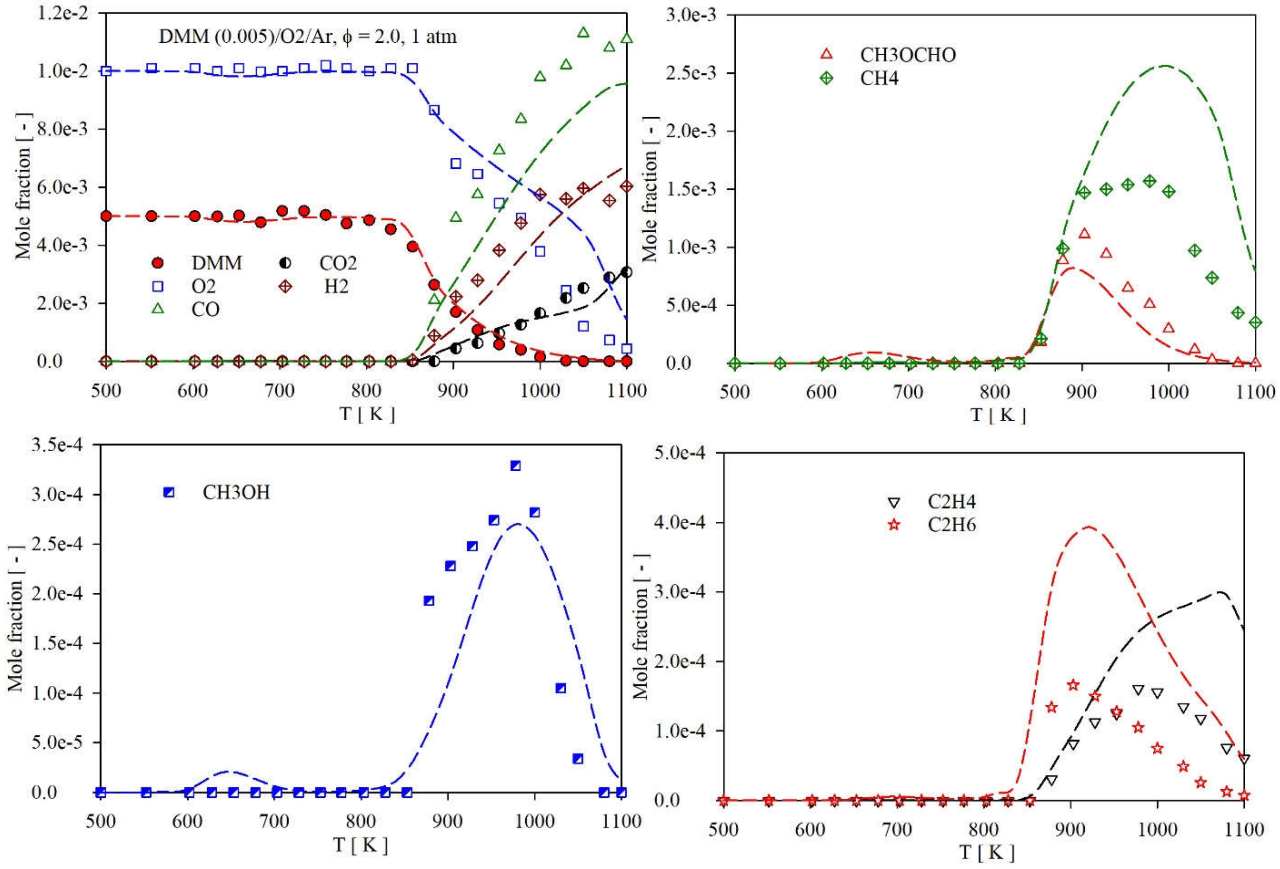

Figure S14: Oxidation of DMM/O_2/Ar in a jet-stirred reactor at 1 atm and ϕ = 2.0. Symbols: experimental data from Gao et al. [6]; lines: this work.

3. Flow reactor

3.1 DME oxidation in a flow reactor

Figures S15 show the temperature dependence of species in a flow reactor at 1 atm and ϕ = 1.06 of DME/O_2/Ar/He blend. The lines in the graph represent the predicted species profiles computed with the proposed model and symbols represent the measurements from [7]. It can be seen in Fig. S15a that the model captures the fuel (DME) consumption as well as predicts major species (CO, CO_2, and H_2) very well. Similar to the JSR the NTC behavior of DME starts at around 600 K and at 960 K DME is completely consumed. For O_2 (Fig. S15b) model over predicts by 28% around 600 K which contradicts the results from a JSR case (Fig. 8a) where the model is in good agreement against the measurements. It is interesting to see that the model predicts H_2O_2 (Fig. S15c) accurately at ~600 K, one of the important low-temperature species, however, at 940 K model overpredicts the H_2O_2 mole fraction by factor 5. Similarly, for formic acid (HOCHO) at ~600 K we can observe the good agreement between model predictions and measurements, however, at a temperature of 950 K model predicts the peak concentration of HOCHO factor 1.5 higher than at 600 K. Measurements at a temperature higher than 850 K were not reported for this species. Furthermore, for CH_4 (Fig. S15e) model predictions and measurements closely agree with each other. For methyl format (CH_3OCHO) the model under predicts by factor 3.5 at ~600 K.

To outline some important reactions during DME oxidation in a flow reactor for the condition shown in Fig. S15 a reaction flow analysis is performed (Fig. S17) at 900 K where 45% of fuel (DME) is consumed. The reaction flow analysis reveals that at this temperature (900 K) all of the DME reacts with OH, CH_3, HO_2, radicals and H-atom forming CH_3OCH_2 radical and respective products. Most of the CH_3OCH_2 (92%) formed mainly undergoes thermal

dissociation channel giving CH_3 and CH_2O, and the reaming recombines with O_2 to give $CH_3OCH_2O_2$. The respective decomposition pathways for CH_3, CH_2O, and $CH_3OCH_2O_2$ are similar to those described in the JSR case (Fig. 9). Additional model validation results for DME oxidation in a flow reactor are shown in Fig. S17 – Fig. S19).

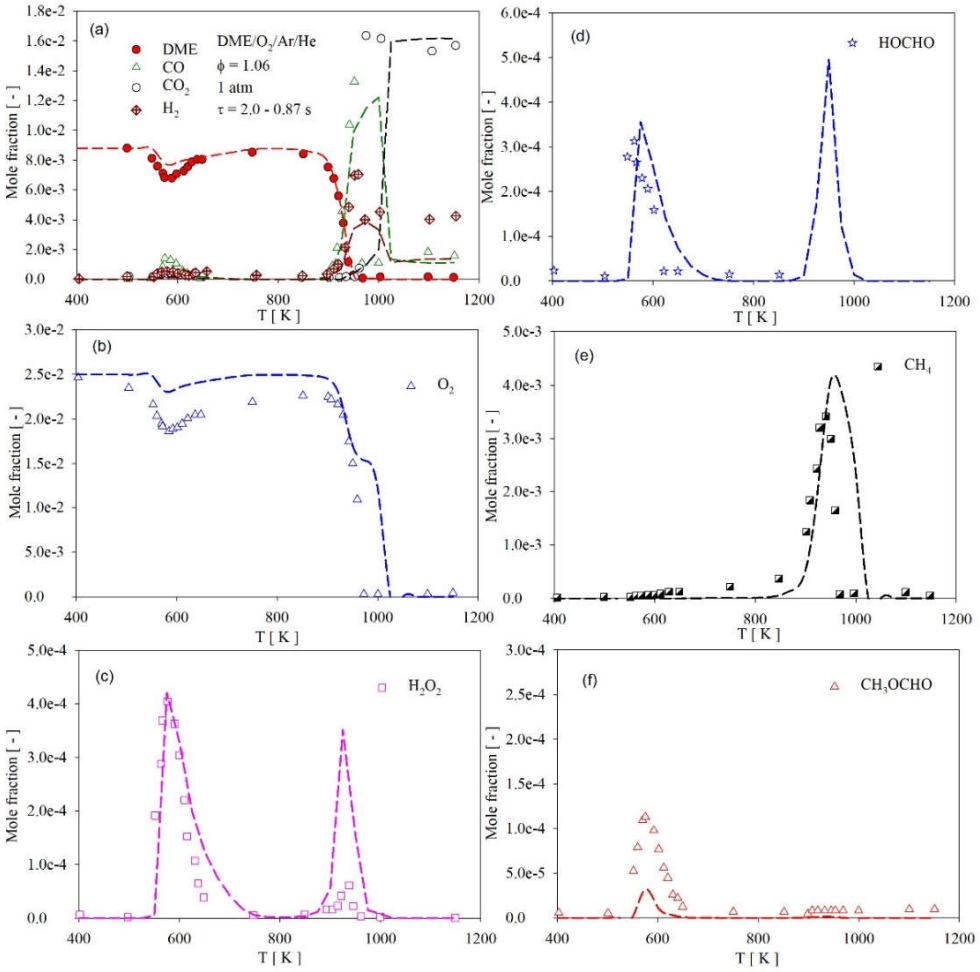

Figure S15: Oxidation of DME/O_2/Ar/He (0.88%/2.5%/2%/94.62 % on a mole basis) in a flow reactor at 1 atm and ϕ = 1.06. Symbols: experimental data from [7], lines: this work.

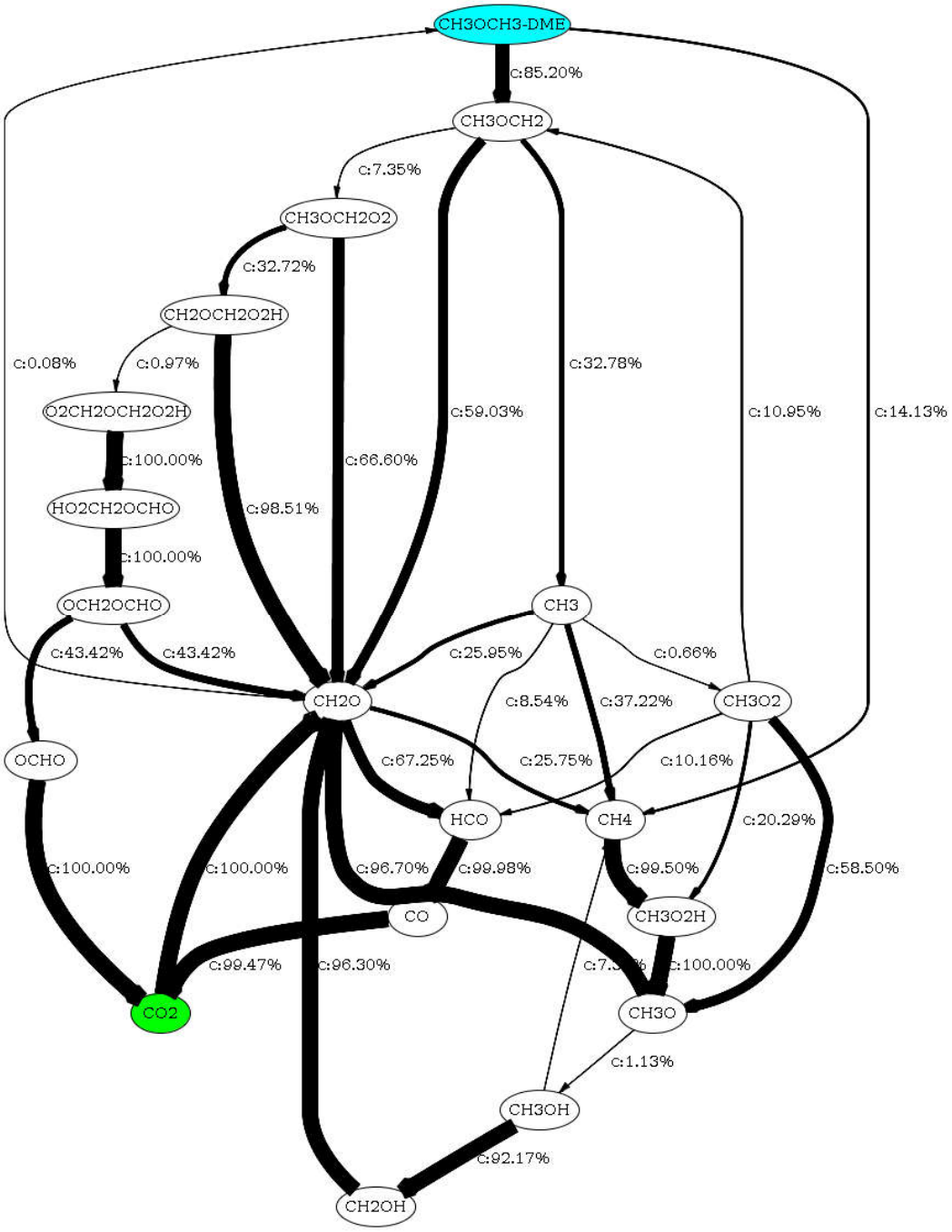

Figure S16: Reaction flow analysis during DME/O_2/Ar/He oxidation in a flow reactor at 900 K for the condition shown in Figure S15.

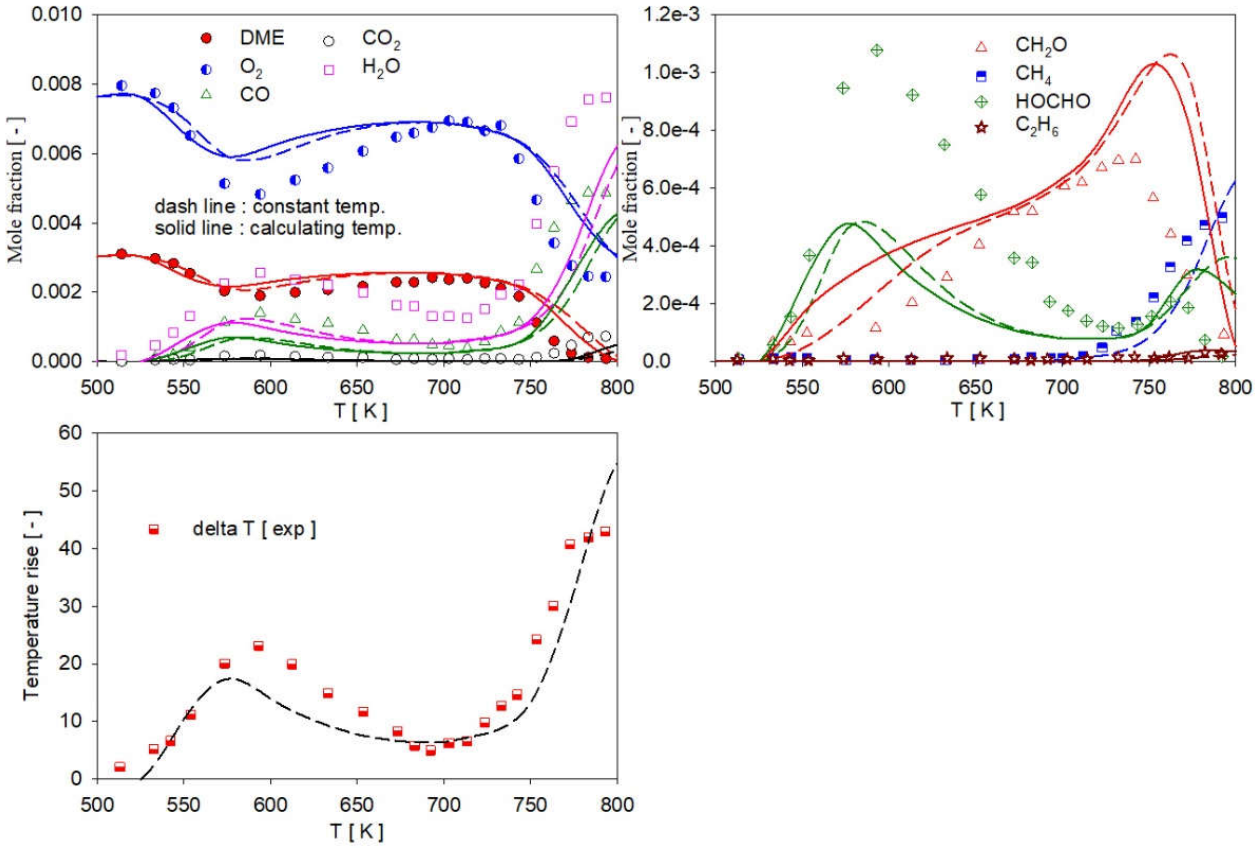

Figure S17: Oxidation of DME/O_2/N2 in a flow reactor at 12.5 atm and ϕ = 1.19. Symbols: experimental data from Curran et al. [8]; lines: this work.

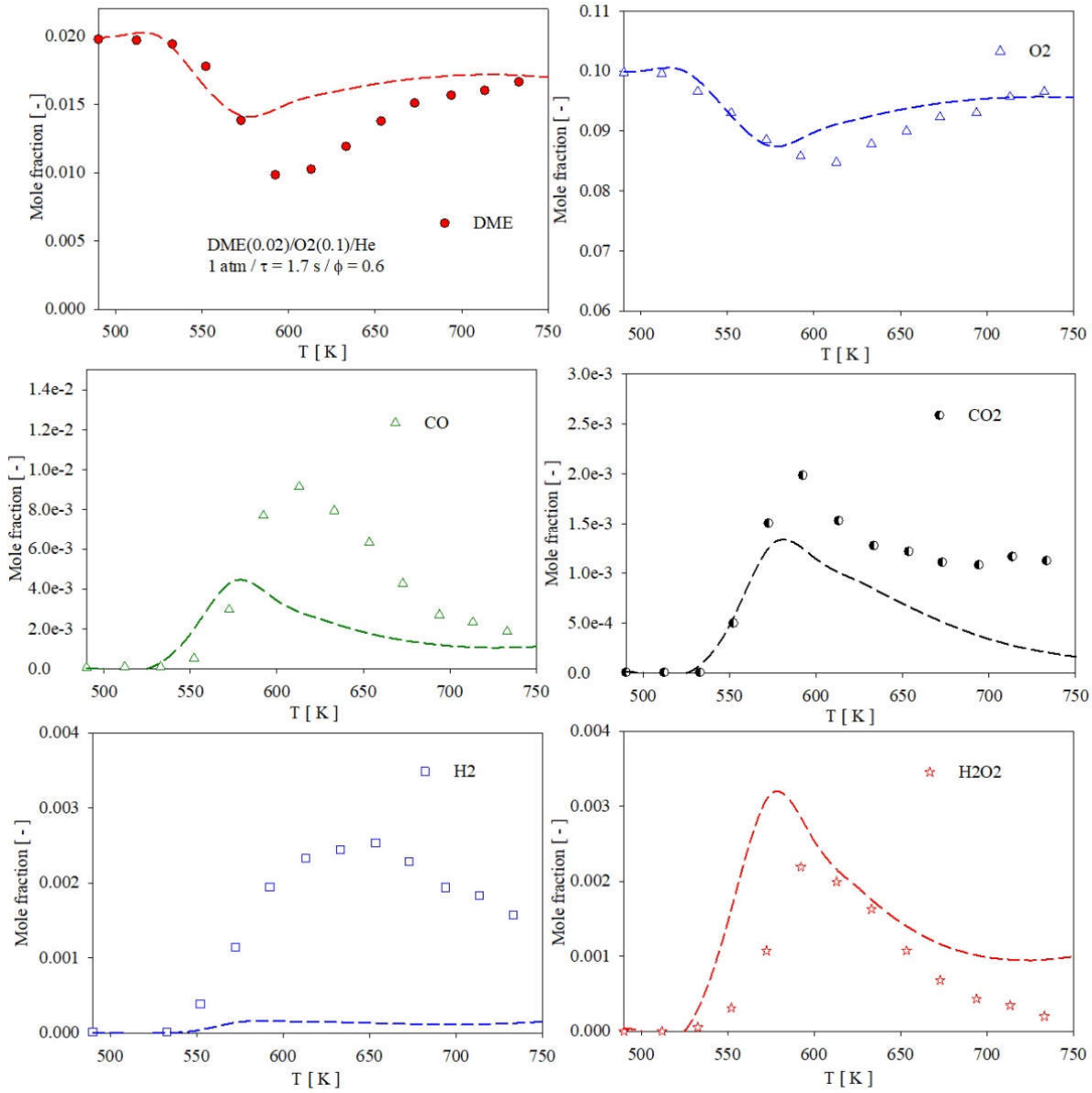

Figure S18: Oxidation of DME/O_2/He in a flow reactor at 1 atm and ϕ = 0.6. Symbols: experimental data from Guo et al. [9]; lines: this work.

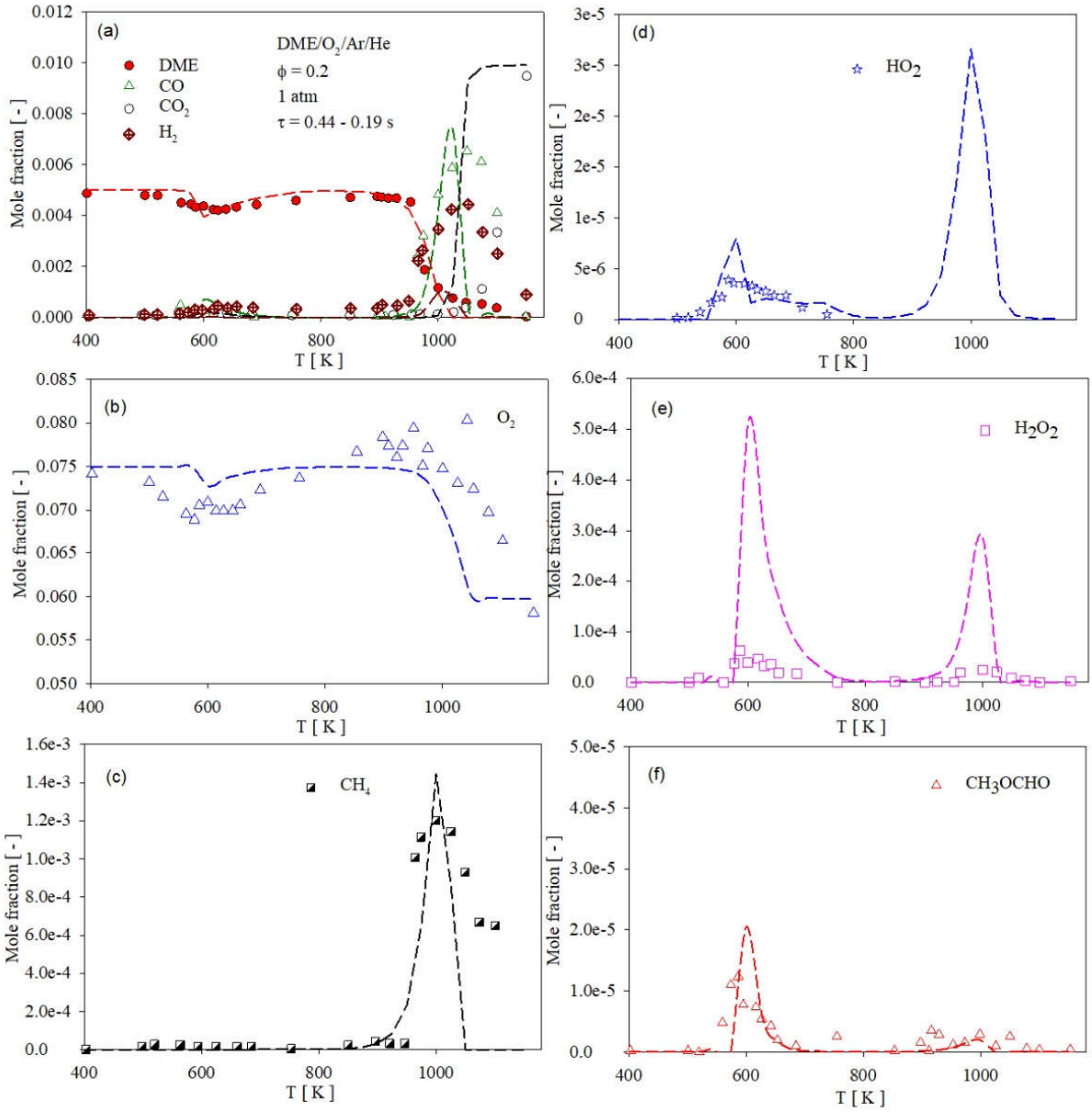

Figure S19: Oxidation of DME/O_2/Ar/He in a flow reactor at 1 atm and ϕ = 0.2. Symbols: experimental data from Kurimoto et al. [7]; lines: this work.

3.2 DMM oxidation in a flow reactor

Figure S20 displays the results of the speciation study (symbols) by Marrodán et al. [10] in a flow reactor during DMM/O_2/N_2 oxidation at 1 atm and ϕ = 1.0. Before any fuel decomposition is observed in the experiment CH_3OH was detected and no comments were made regarding this by

authors in their work [10]. To capture this early formation of CH_3OH in simulation a small amount of CH_3OH ($1.3x10^{-5}$ mole fraction) was added in the initial mixture. A simulation without CH_3OH in the initial mixture is also performed (see Fig. S21) and similar results are obtained. As can be seen, the onset temperature for DMM consumption is well predicted by the model (Figure S20a) further demonstrating its robustness. However, the model predicts the fuel consumption temperature consistently 20 K lower than that of the experimental data over the temperature range of 1020 and 1070 K. The complete consumption of DMM happens at ~1070 K, which is ~100 K higher than observed for DME case (Figure S15). Similar to that observed in JSR (Figure 11a), flow reactor data also reveals that DMM does not show any NTC behavior which is contrary to DME (Figure S15a). As for the major species (CO, CO_2, and H_2), our kinetic model show excellent predictability capacity of the onset temperature for their formation. Among these species, the peak mole fraction of CO is underpredicted by ~24%. It can be observed in Figure S20b model overpredicts CH_3OH peak mole fraction ~50% and underpredicts the CH_3OCHO peak mole fraction by ~33%, which is contrary to the case of JSR (Figure 11). Similarly, for other intermediates species CH_4 (Figure S20c) and C_2H_4 (Figure S20d) model predicts the peak mole fraction very well while C_2H_6 (Figure S20d) is overpredicted by factor 2. Overall, model performance is satisfactory for the conditions shown in Figure S20.

A reaction flow analysis at 1000 K (see Fig. S22, where 41% of the fuel is consumed) reveals that DMM mainly reacts with H-atoms, OH and CH_3 radicals to give $CH_3OCH_2OCH_2$ (R1) and $CH_3OCHOCH_3O$ (R2) radicals while the highest contribution is made by H-atom and least is made by CH_3. The reaction path forming R1 is favored more (by 6%) compared to path forming R2. The remaining DMM undergoes thermal dissociation forming DME, CH_3OCH_2, CH_3OH, CH_2O, HCO,

and CH_3 *via* the reactions r2, r3, and r4 respectively. The degradation pathways of radicals R1 and R2 formed in the above process are the same as shown in Figure 12.

We made no further attempts to optimize the model for a better description of the flow reactor data for both DME and DMM. We note that to date the only published experimental data in a flow reactor experiment for DMM are from [10,11]. Future experimental study on DMM from different facilities are highly desirable to provide further insights into DMM oxidation in a flow reactor environment. Additional model validation for DMM oxidation in a flow reactor is shown in Fig. S23 – Fig. S24.

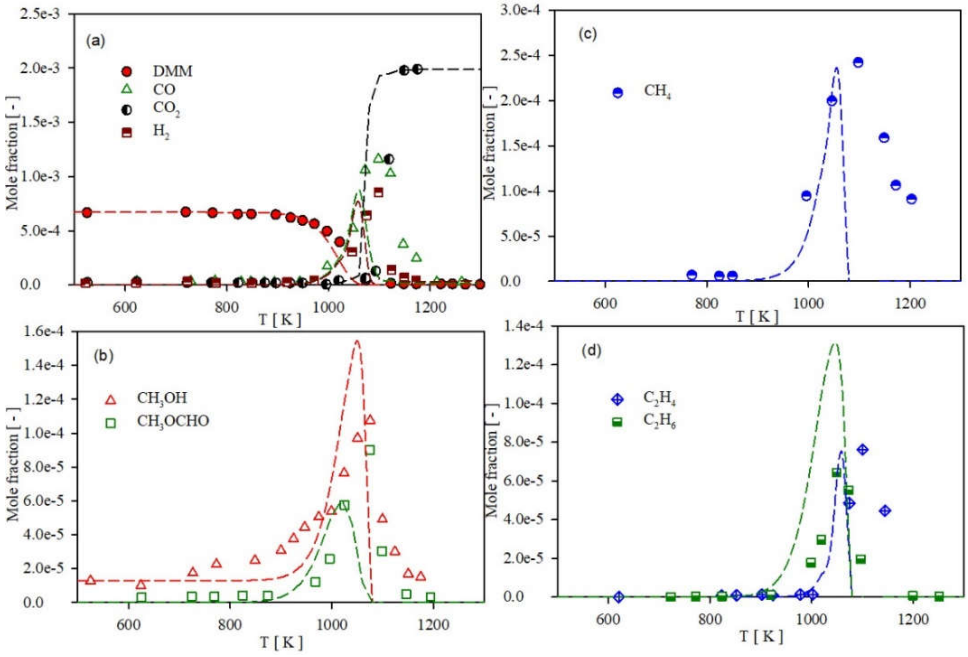

Figure S20: Oxidation of DMM/O_2/N_2 in a flow reactor at 1 atm, ϕ = 1.0 and τ (s) = 195/T(K). Symbols: experimental data from [10], lines: this work. CH_3OH (1.3×10^{-5} mole fraction) added in initial mixture for simulation.

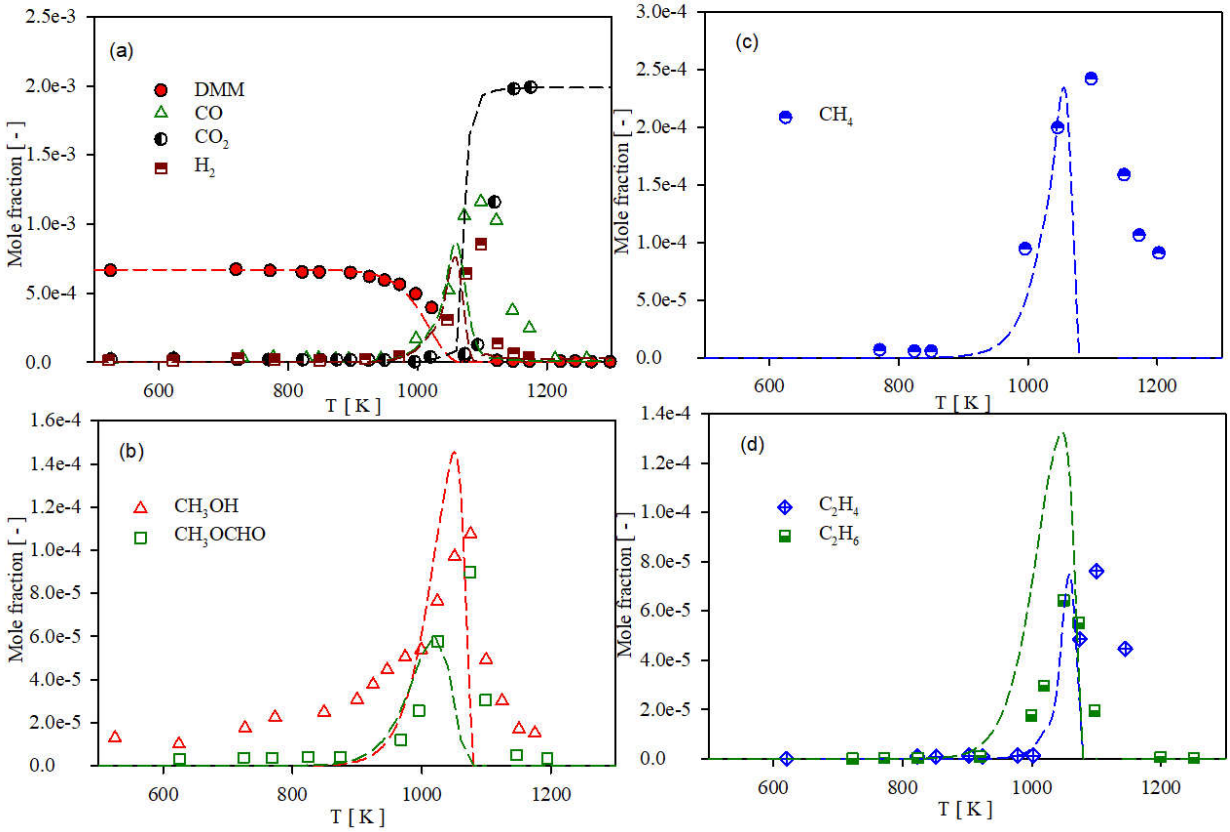

Figure S21: Oxidation of DMM/O_2/N_2 in a flow reactor at 1 atm, ϕ = 1.0 and τ (s) = 195/T(K). Symbols: experimental data from Marrodán et al. [10], lines: this work.

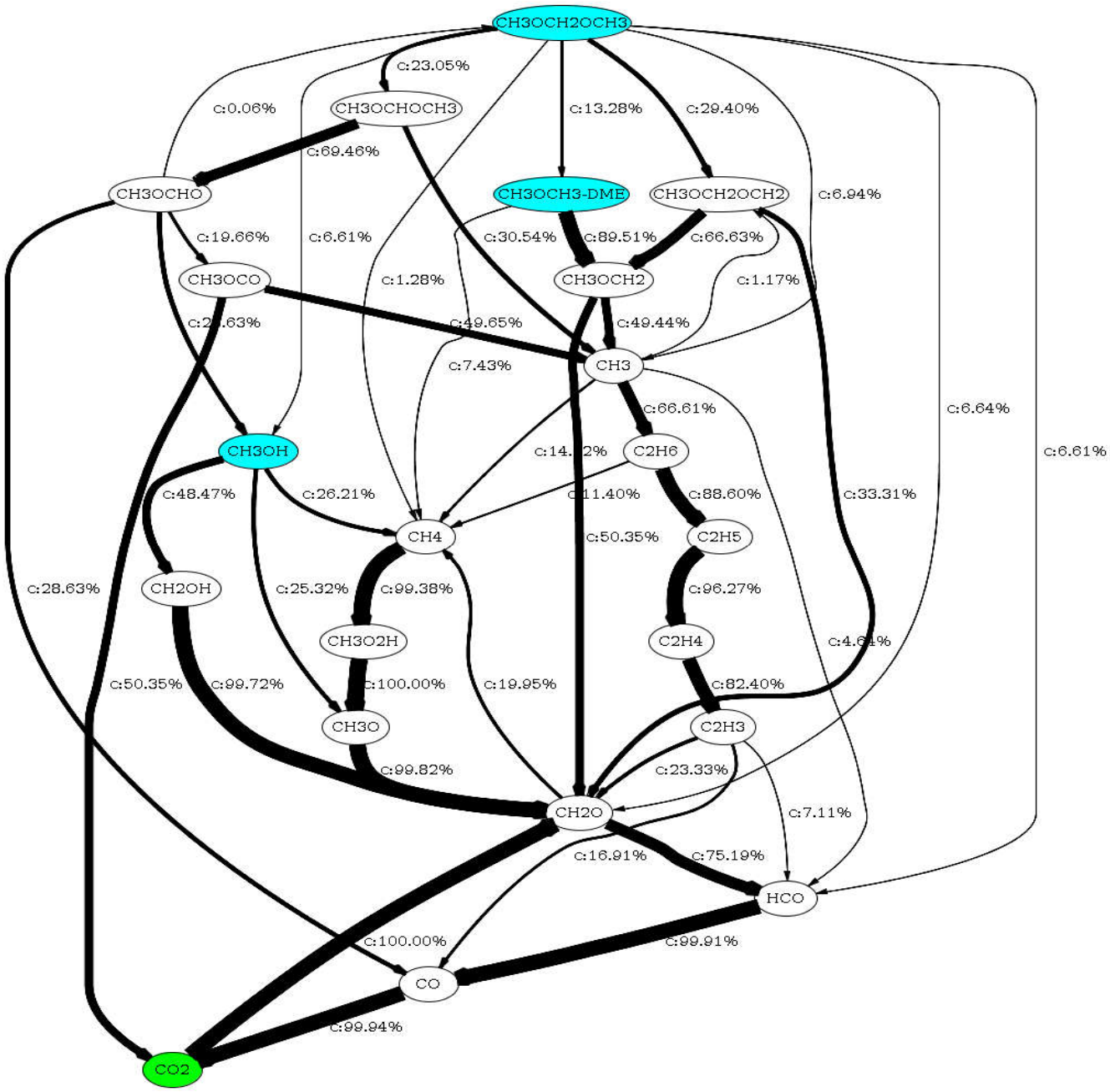

Figure S22: Reaction flow analysis during DMM/O_2/N_2 oxidation in a flow reactor at 1000 K for the condition shown in Figure 15.

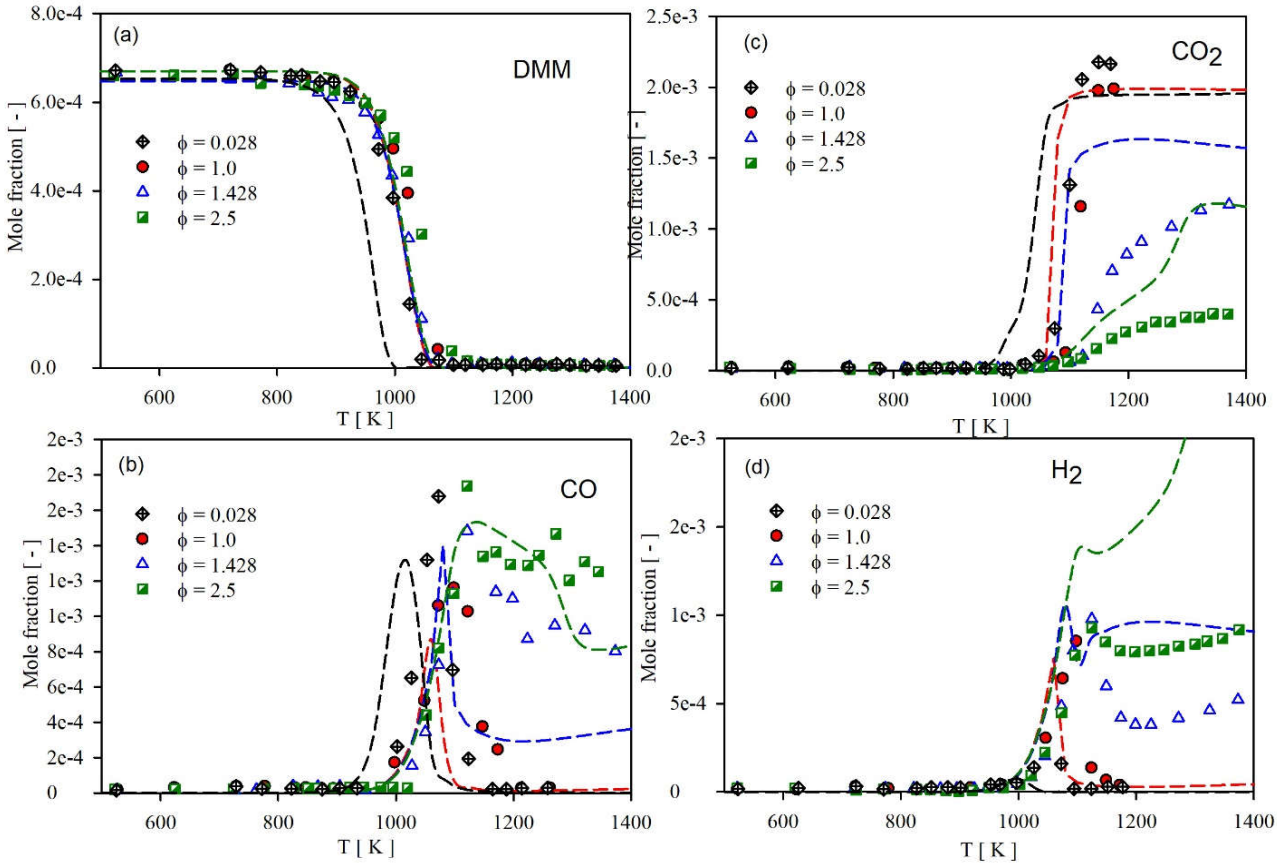

Figure S23: Oxidation of DMM/O_2/N_2 in a flow reactor at 1 atm and different ϕ, for residence time τ (s) = 195/T(K). Symbols: experimental data from Marrodán et al. [10]; lines: this work.

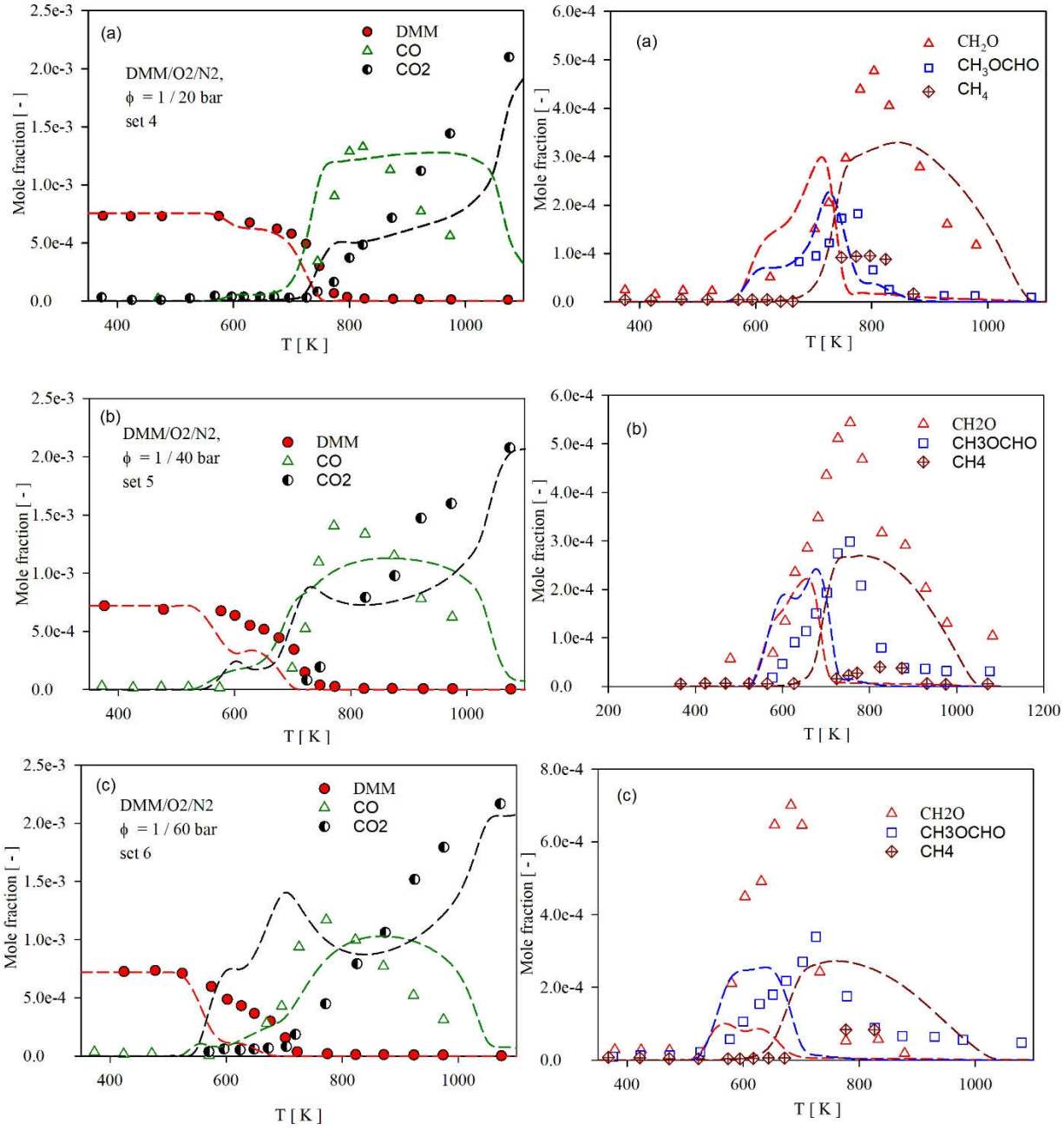

Figure S24: Oxidation of DMM/O_2/N_2 in a flow reactor at ϕ = 1.0 and different pressure (20, 40 and 60 bar). Symbols: experimental data from Marrodán et al. [11]; lines: this work.

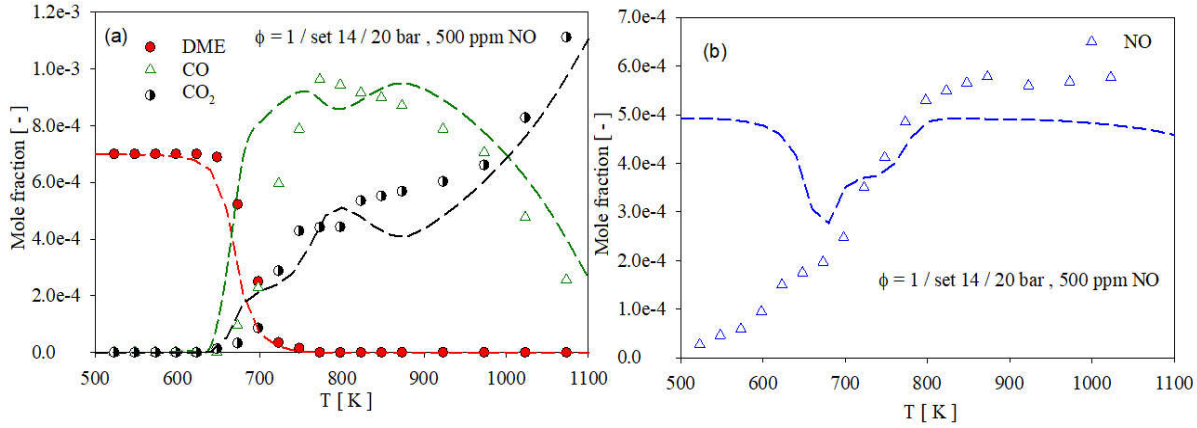

Figure S25: Oxidation of DME/O_2/N2/NO(500 ppm) in a flow reactor at 20 bar and ϕ = 1.0. Symbols: experimental data from Marrodán et al. [12]; lines: this work

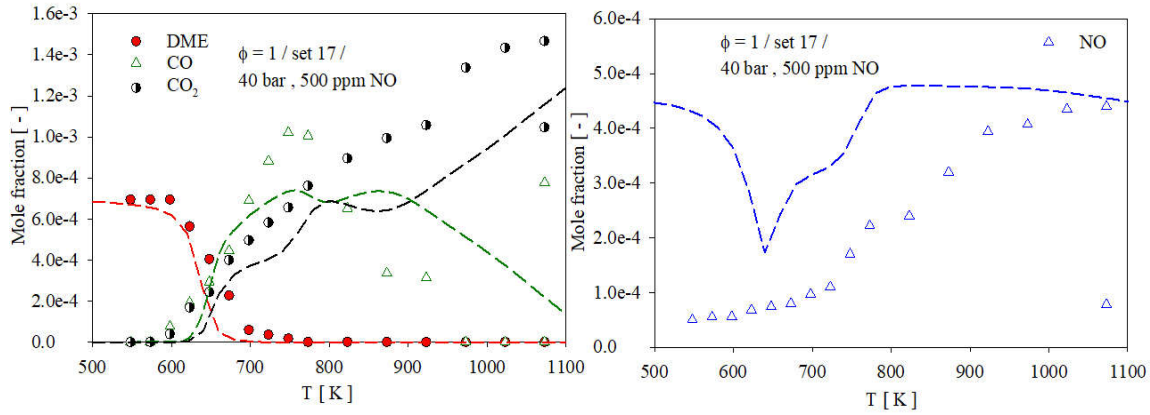

Figure S26: Oxidation of DME/O_2/N2/NO(500 ppm) in a flow reactor at 40 bar and ϕ = 1.0. Symbols: experimental data from Marrodán et al. [12]; lines: this work.

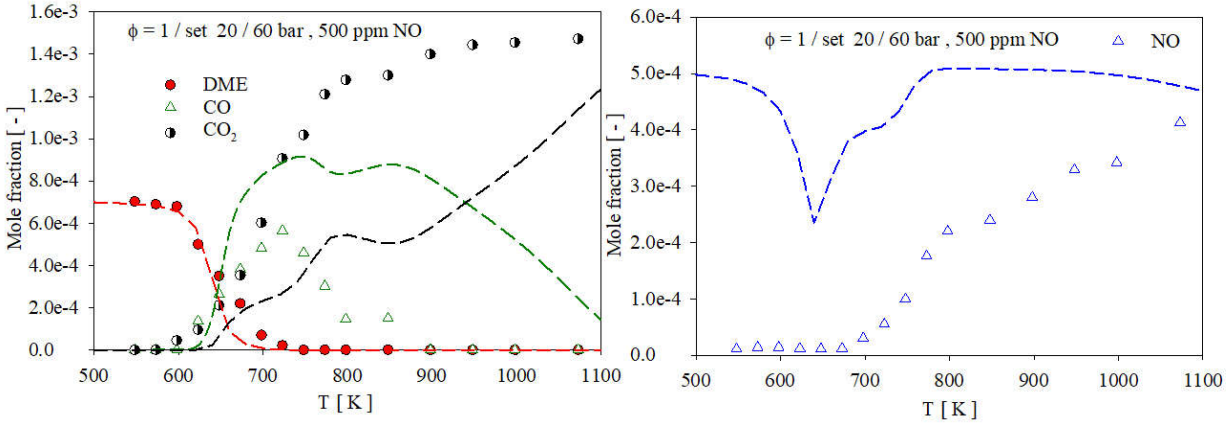

Figure S27: Oxidation of DME/O_2/N2/NO(500 ppm) in a flow reactor at 60 bar and ϕ = 1.0. Symbols: experimental data from Marrodán et al. [12]; lines: this work.

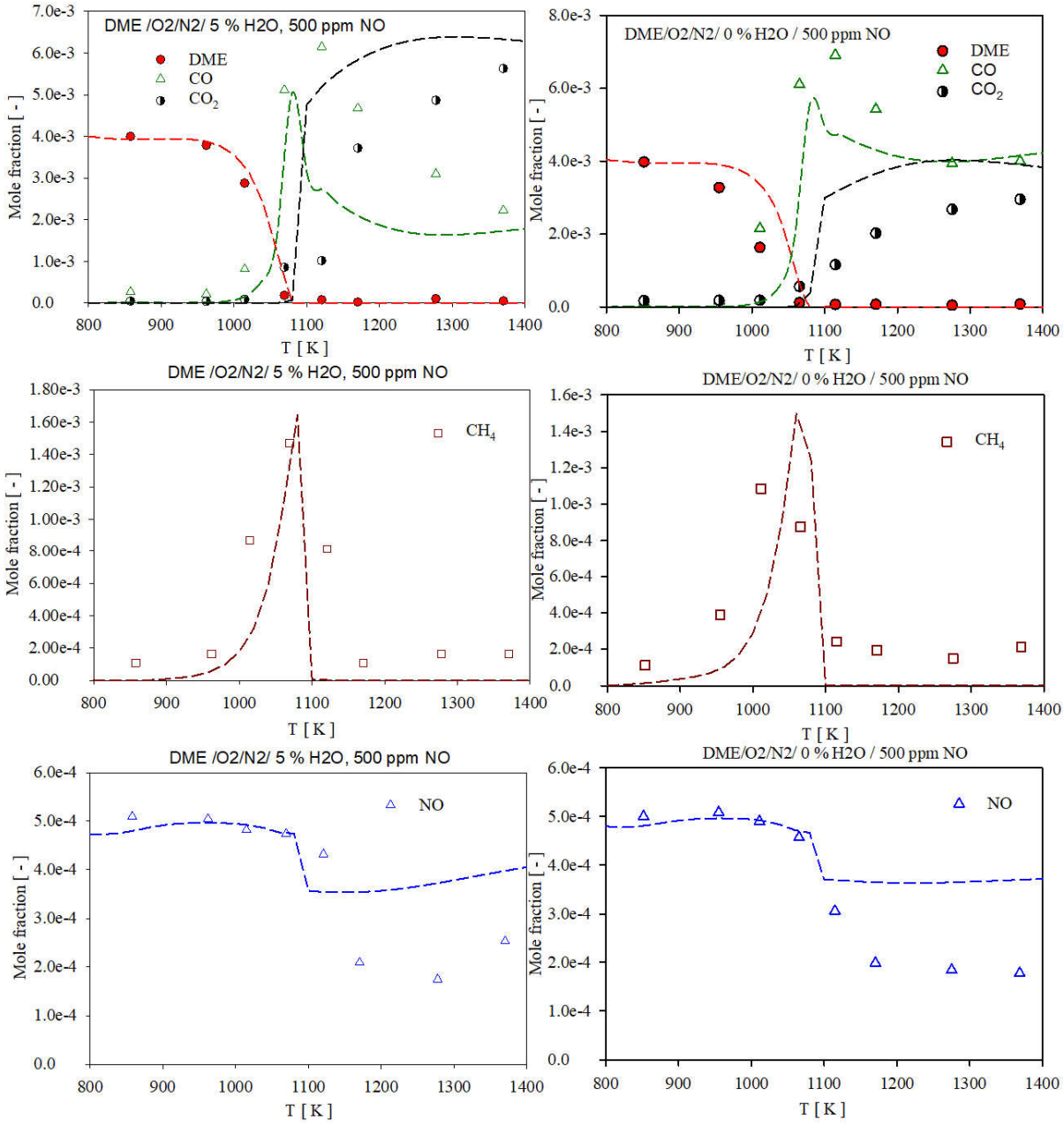

Figure S28: Oxidation of DME/O_2/N_2/H_2O/NO (500 ppm) in a flow reactor at 1 atm with 5 % H_2O (left), with no H_2O (right). Symbols: experimental data from Yamamoto et al. [13]; lines: this work.

3 Burner stabilized flame

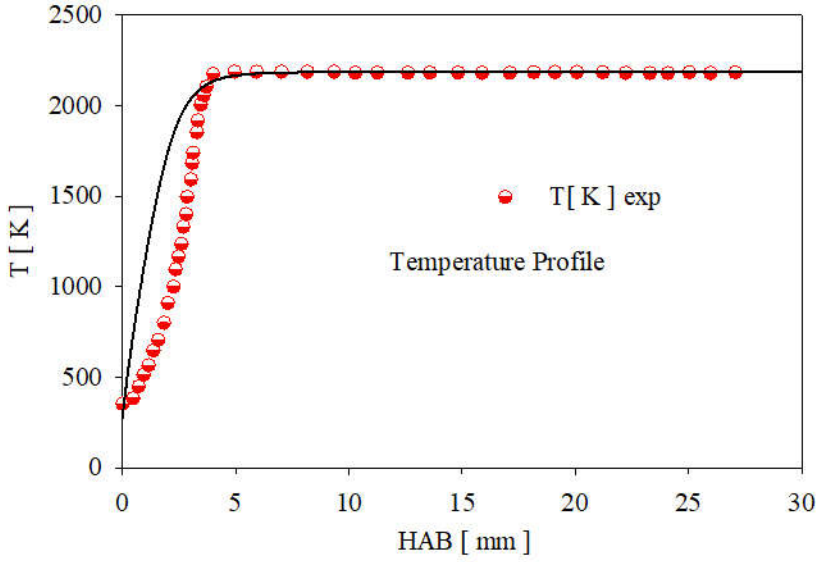

Figure S29: Temperature profile of DME/O_2/Ar (0.17582/0.32418/0.5, mole fraction) burner stabilized premixed flame at 5 kPa and ϕ = 1.63 for flame shown in Fig. 17. Symbols: experimental measured temperature profile [14], line: calculated temperature profile solving the energy conservation equation.

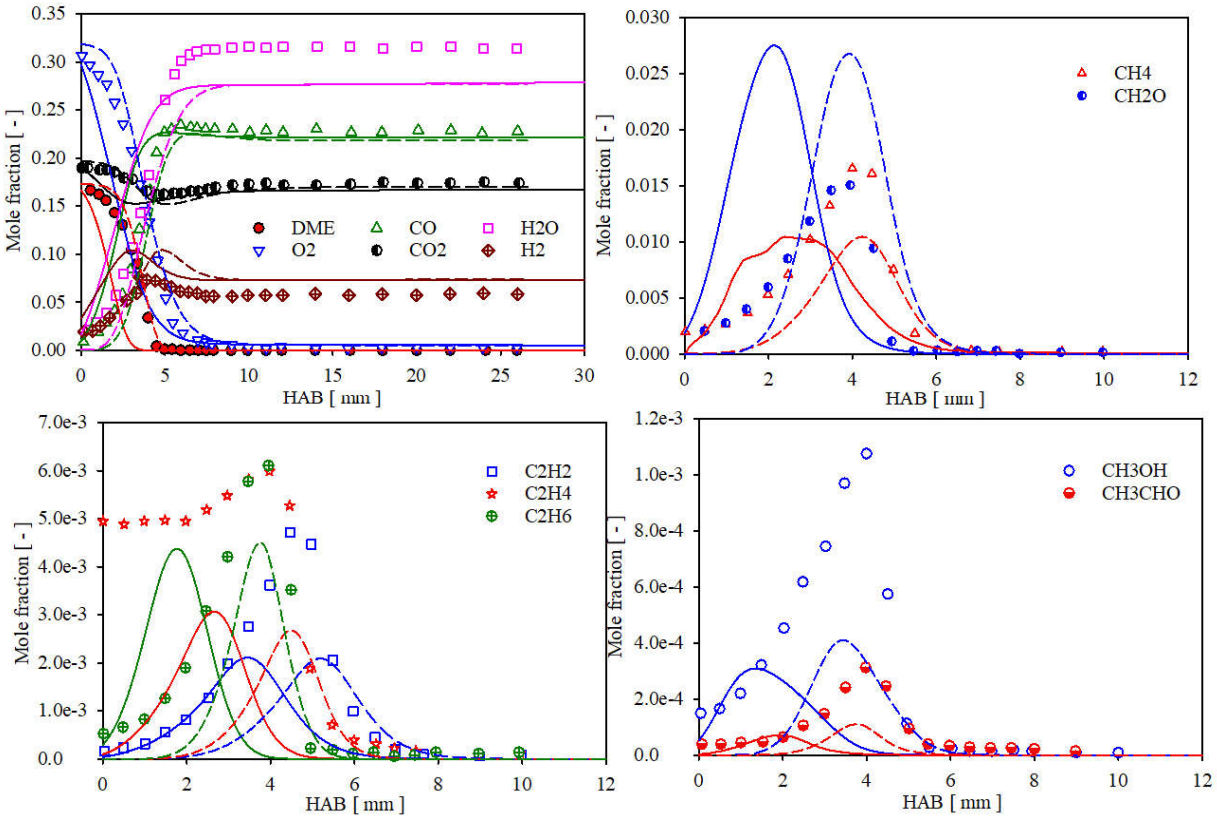

Figure S30: Speciation of DME/O_2/Ar/CO_2 premixed flame at ϕ = 1.63, 5 kPa. Symbols: experimental data from Liu et al. [14], lines: this work. Dashed lines: imposing experimental temperature profile, solid lines: solving energy conservation equation.

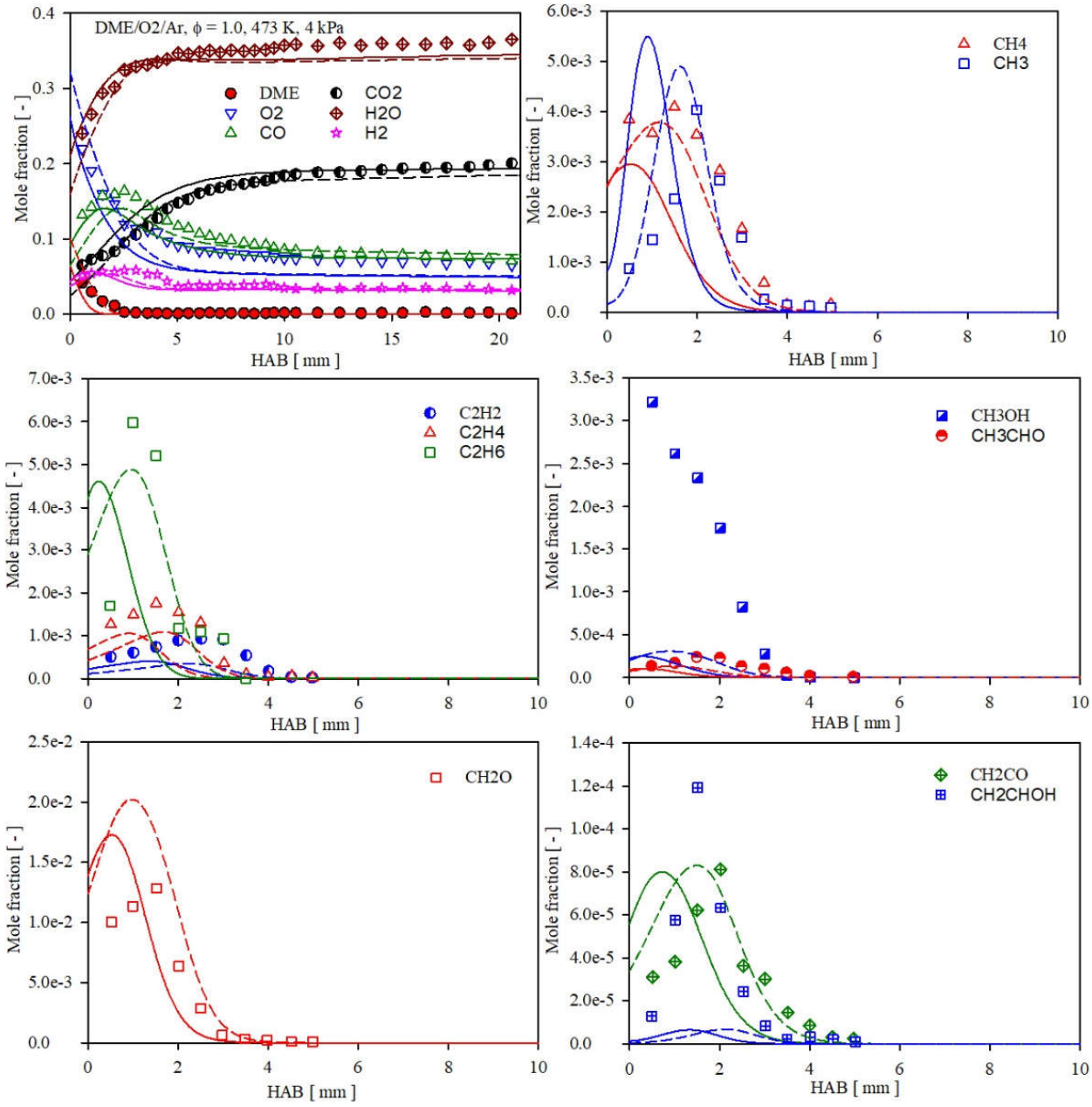

Figure S31: Speciation of DME/O_2/Ar premixed flame at ϕ = 1.0, 4 kPa, 473 K. Symbols: experimental data from Xu et al. [15]; lines: this work. Dashed lines: imposing experimental temperature profile, solid lines: solving energy conservation equation.

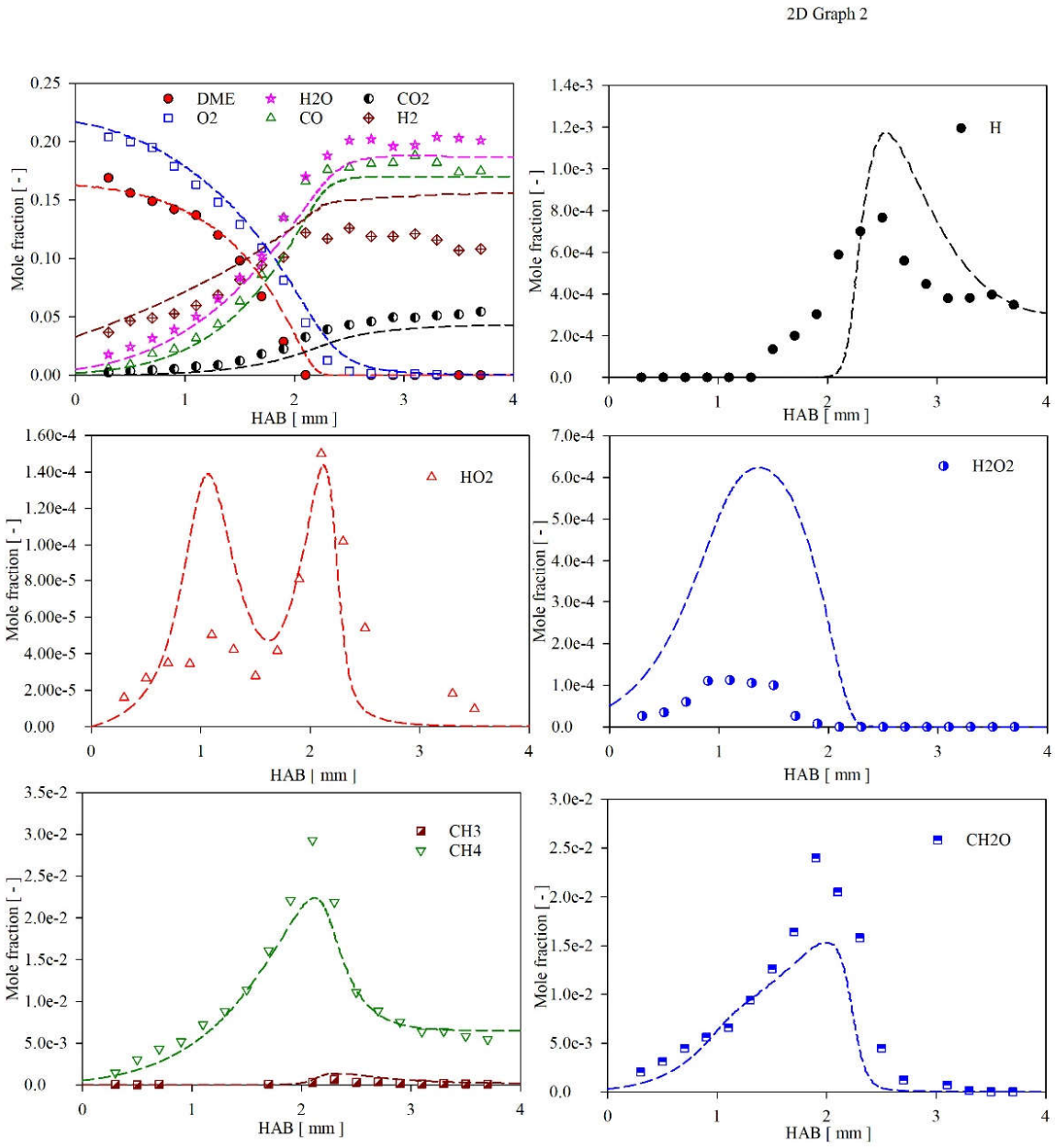

Figure S32: Speciation of DME/O_2/Ar premixed flame at ϕ = 2.2, 1 atm, 368 K. Symbols: experimental data from Bolshova et al. [16]; lines: this work. Dashed lines: imposing experimental temperature profile.

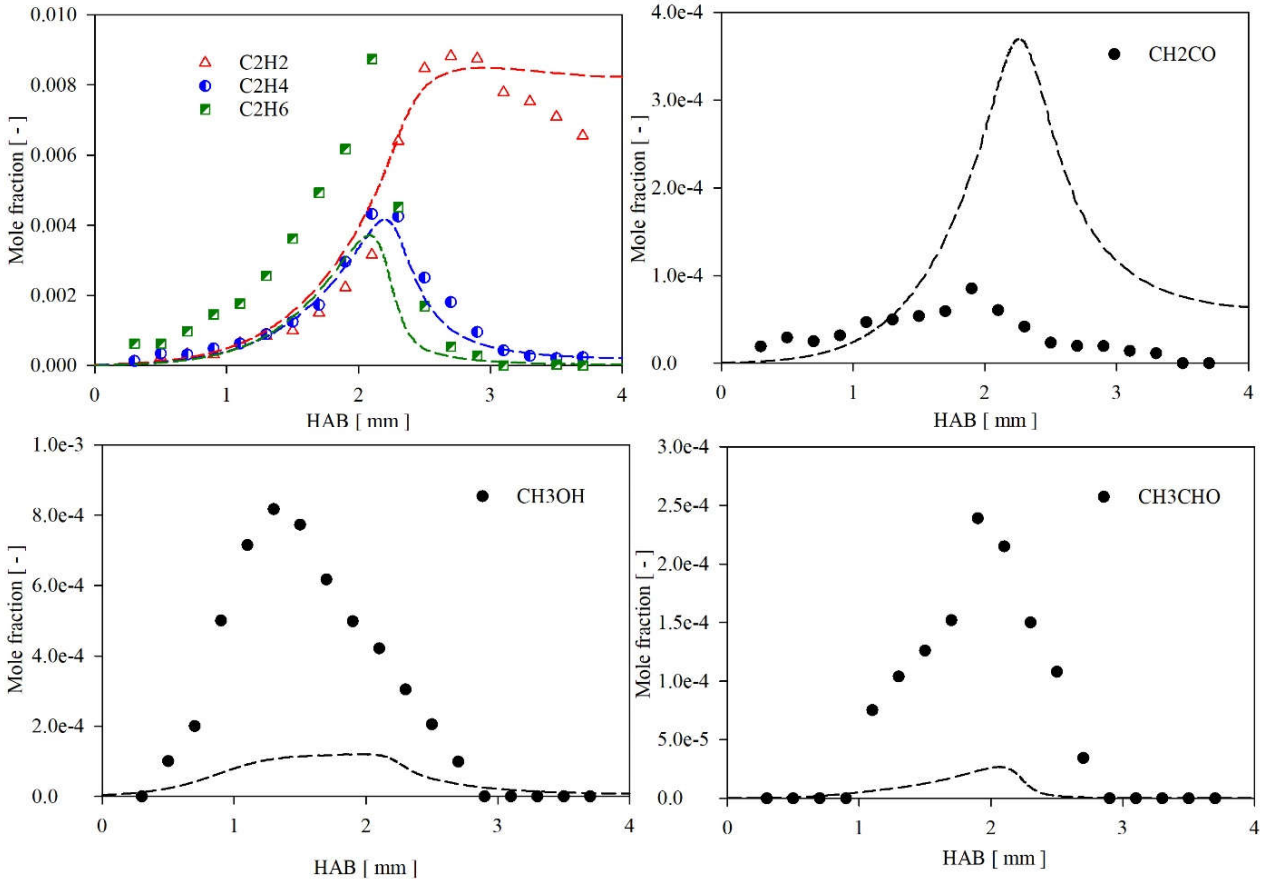

Figure S33: Speciation of DME/O_2/Ar premixed flame (Figure S17) at ϕ = 2.2, 1 atm, 368 K. Symbols: experimental data from Bolshova et al. [16]; lines: this work. Dashed lines: imposing experimental temperature profile.

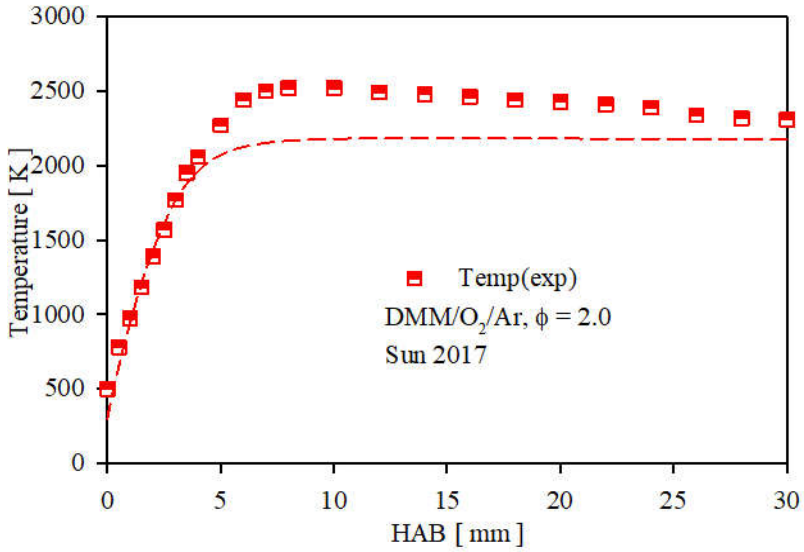

Figure S34: Temperature profile of DMM/O_2/Ar (0.25/0.50/0.25, mole fraction) burner stabilized premixed flame at 4 kPa and $\phi = 2.0$ for flame shown in Fig. 19. Symbols: experimental measured temperature profile [17], line: calculated temperature profile solving the energy conservation equation.

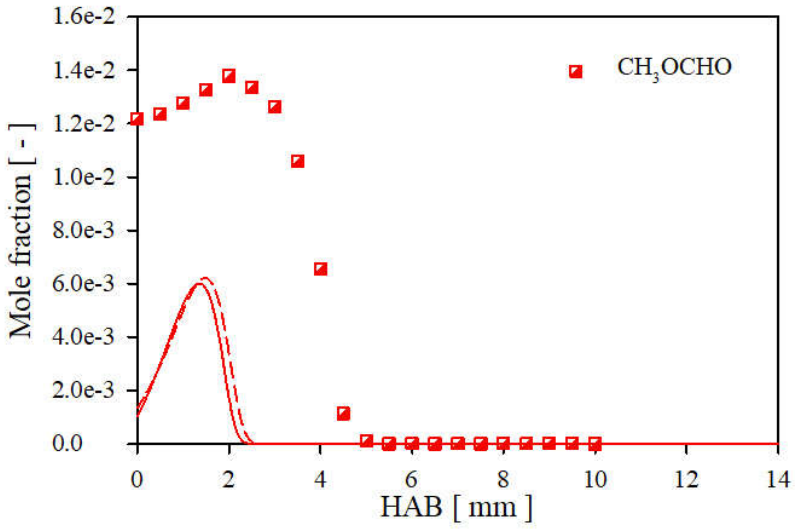

Figure S35: Speciation in a DMM($CH_3OCH_2OCH_3$)/O_2/Ar (0.25/0.5/0.25, mole fraction) burner stabilized premixed flame at 4 kPa and $\phi = 2.0$ for flame shown in Fig. 19. Symbols: experimental data from Sun et al. [17], lines: this work. Dashed lines: prediction imposing experimental temperature profile, solid lines: prediction solving energy conservation equation.

4 Ignition delay time

4.1 DME/air reaction sensitivity analysis for Figure 19

Figure S36 displays the normalized reaction sensitivity analysis at 800 K, 23 bar and ϕ = 1.0 for DME/air ignition delay time. In Figure S36 positive sensitivity means reaction promotes system reactivity (decreased IDT), and negative sensitivity means reaction retards reactivity (increased IDT). It can be observed that the highest sensitivity is exhibited by a reaction of DME with HO_2. This reaction was also seen in the sensitivity analysis during DME oxidation in JSR (see Figure 10) exhibiting the highest sensitivity, which is expected, as reactions with HO_2 radicals at low temperatures are important. Furthermore, it can be observed that the reaction of DME with H-atom or CH_3 (CH_3OCH_3-DME+H/CH_3=CH_3OCH_2+H_2/CH_4) show a decreased sensitivity compared to reactions with OH radicals. In the results from section 5.2 and 5.4 for DME oxidation, it was found that CH_2O is one of the major intermediate species at low and high temperatures. In line with those findings reactions involving CH_2O are also among the most sensitive reactions for IDT prediction (see Figure S36, CH_2O+OH/HO_2=HCO+H_2O/H_2O_2). Furthermore, in Figure S36 it can be observed that most of the reactions involve HO_2 and OH radical indicating the importance of these species at low temperatures.

Reaction sensitivity analysis at 1100 K is also performed (see Fig. S37). The reaction (CH_3OCH_3-DME+CH_3=CH_3OCH_2+CH_4) which exhibited a low sensitivity at 800 K (Figure S36) now exhibits the highest sensitivity. Similar observations can be drawn for other important reactions from Figure S36 and Figure S37. Further model validation for DME ignition delay times using other published experiments is shown Fig. S38.

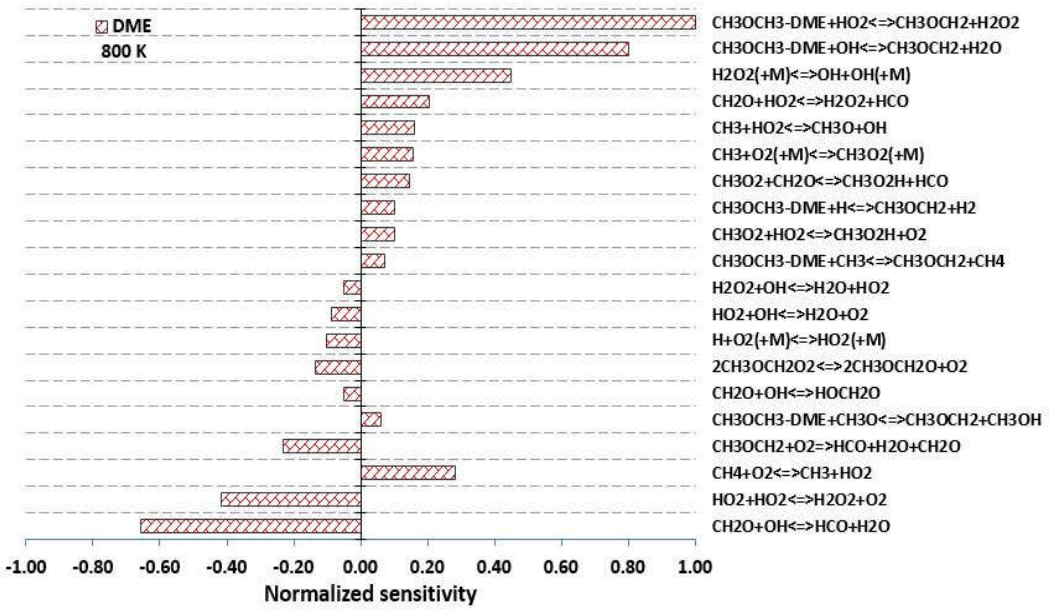

Figure S36: Normalized reaction sensitivity towards ignition delay time at 800 K, 23bar, $\phi = 1.0$ for DME/air.

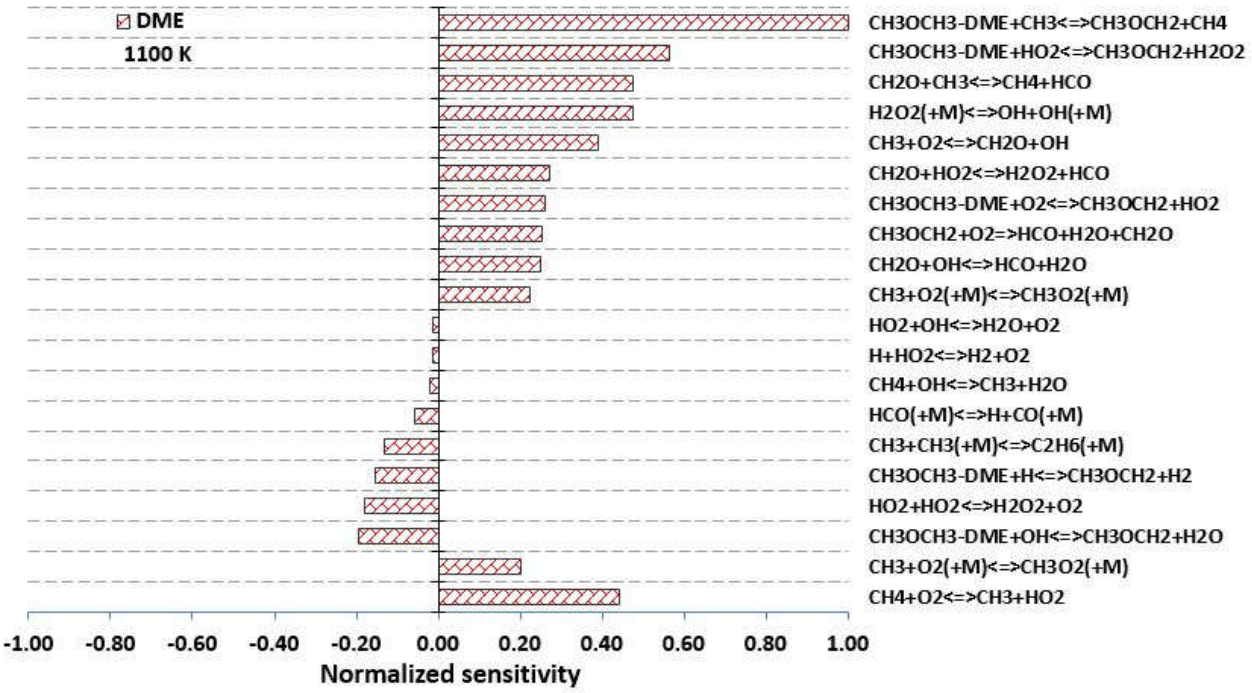

Figure S37: Normalized reaction sensitivity towards ignition delay time at 1100 K, 23 bar, ϕ = 1.0 for DME/air.

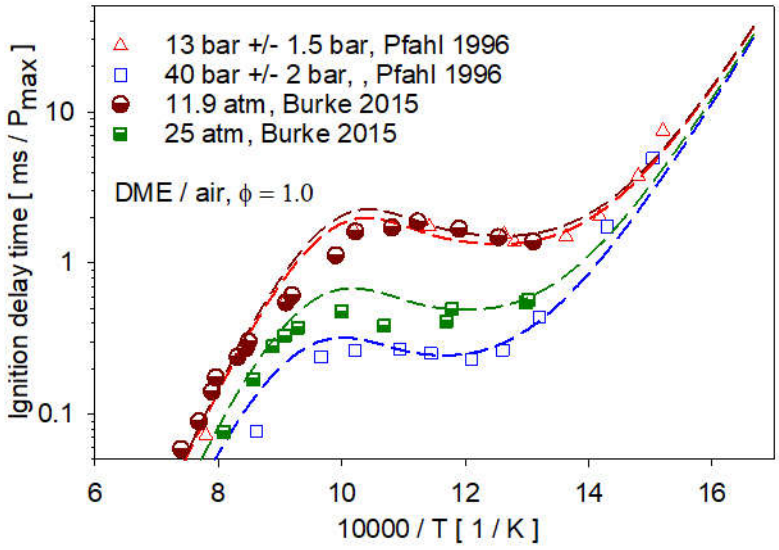

Figure S38: Ignition delay time of DME/air at ϕ = 1.0 and different pressure in a shock tube. Symbols: experimental data from [18,19]; lines: this model.

4.2 DMM/air reaction sensitivity analysis for Figure 20

Figure S39 displays the normalized reaction sensitivity at 800 K, 20 bar and ϕ = 1.0 for DMM/air ignition delay time. The sensitivity direction implies the same meaning as mentioned above for DME (Figure S36). The highest sensitivity is exhibited by the H-atom abstraction reactions by OH radical (r9 and r10). However, reaction r9 displays positive sensitivity while reaction r10 shows negative sensitivity. These reactions were also among the most sensitive reaction for DMM oxidation in JSR (see section 5.2). Similarly, reactions of DMM with HO_2 (r11 and r12) are also among the sensitive reactions. In contradiction with reaction r9 and r10 both of these reactions display positive a sensitivity. As discussed in section 3, the reaction of DMM with CH_3O_2 (r13 and r14) was found to be important for predicting the ignition delay time mainly in the low to intermediate temperature transition region. In Figure S39, we can observe that these reactions are among the most sensitive reactions and both exhibit positive sensitivity. In line with the above finding, the recombination reaction forming CH_3O_2 ($CH_3+O_2(+M)=CH_3O_2(+M)$) appears as a sensitive reaction. Interestingly in the case of DME, the reaction of CH_3O_2 with DME (Figure S36) at the same temperature does not appear in sensitivity analysis, though reaction $CH_3+O_2(+M)=CH_3O_2(+M)$ appears and exhibits positive sensitivity for both fuels (DME and DMM) IDT.

Reaction sensitivity analysis at a temperature of 1100 K is also performed (see Fig. S40). Sensitivity analysis reveals that recombination reaction ($CH_3+O_2(+M)=CH_3O_2(+M)$) has the highest sensitivity. At this temperature also reactions of DMM with CH_3O_2 (r13 and r14) are among the most sensitive reactions. This indicates the increased importance of CH_3O_2 species and the reactions involving it for DMM oxidation. Similar comparison and observation can be drawn

for other reactions from Figure S39 and Fig. S40. Additional model validation for DMM ignition delay times using other published experiments is shown in Figure S41.

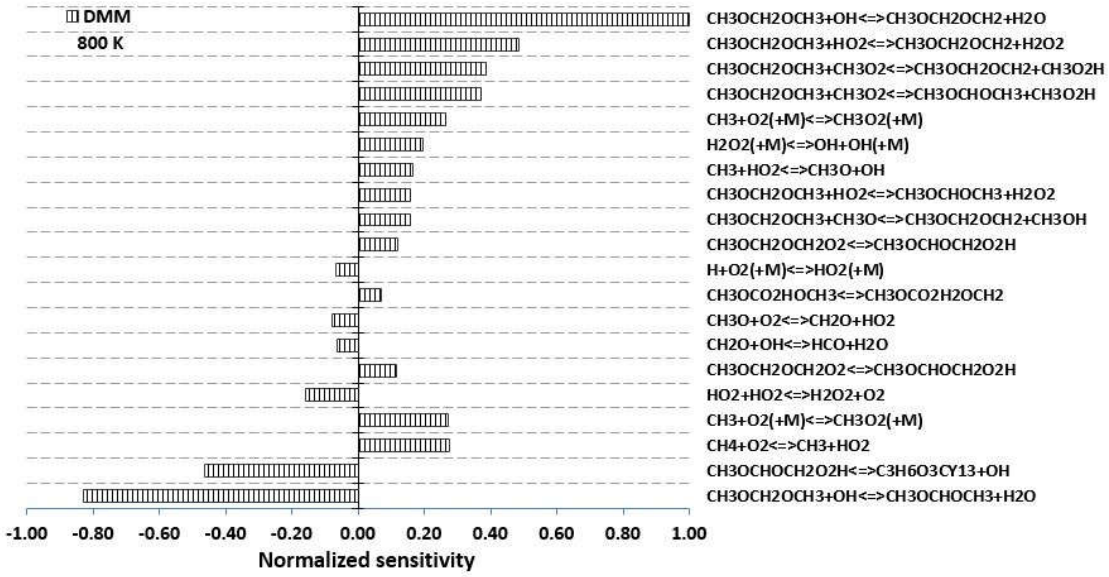

Figure S39: Normalized reaction sensitivity towards ignition delay time at 800 K, 20 bar, ϕ = 1.0 for DMM/air.

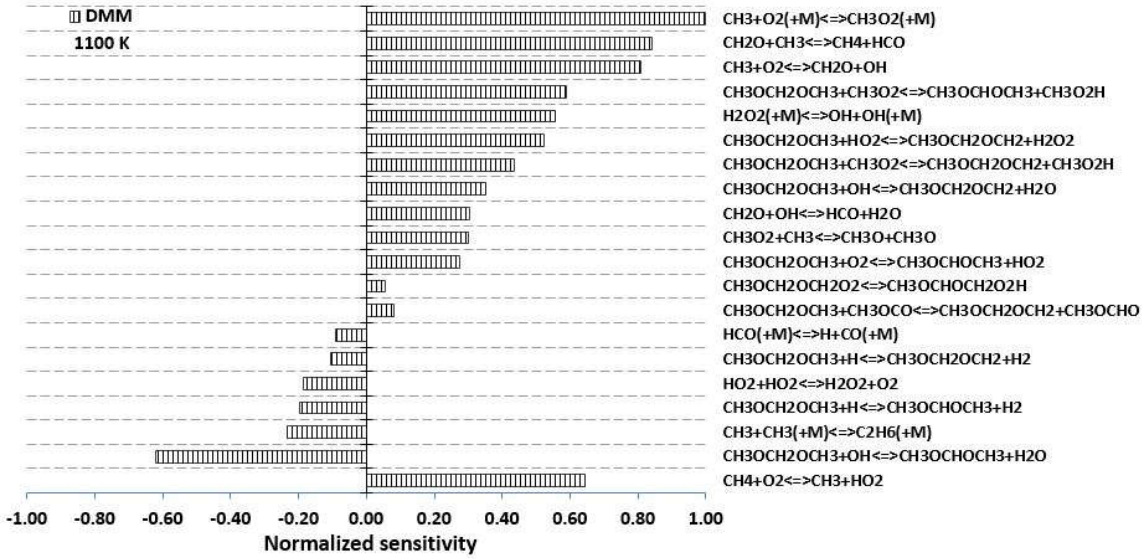

Figure S40: Normalized reaction sensitivity towards ignition delay time at 1100 K, 20 bar, ϕ = 1.0 for DMM/air.

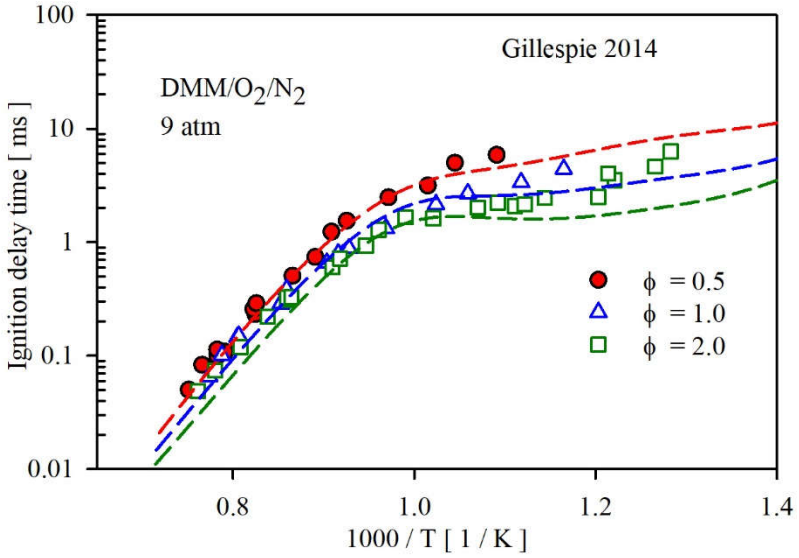

Figure S41: Ignition delay time of DMM/air at 9 atm bar and different equivalence ratio in a shock tube. Symbols: experimental data from Gillespie et al. [20]; lines: this model.

References

[1] X. Qin, Y. Ju, Measurements of burning velocities of dimethyl ether and air premixed flames at elevated pressures, Proc. Combust. Inst. 30 (2005) 233–240. doi:10.1016/j.proci.2004.08.251.

[2] R.J. Varghese, V.R. Kishore, M. Akram, Y. Yoon, S. Kumar, Burning velocities of DME(dimethyl ether)-air premixed flames at elevated temperatures, Energy. 126 (2017) 34–41. doi:10.1016/j.energy.2017.03.004.

[3] A. Rodriguez, O. Frottier, O. Herbinet, R. Fournet, R. Bounaceur, C. Fittschen, F. Battin-Leclerc, Experimental and Modeling Investigation of the Low-Temperature Oxidation of Dimethyl Ether, J. Phys. Chem. A. 119 (2015) 7905–7923. doi:10.1021/acs.jpca.5b01939.

[4] P. Dagaut, C. Daly, J.M. Simmie, M. Cathonnet, The oxidation and ignition of dimethylether from low to high temperature (500-1600 K): Experiments and kinetic modeling, in: Symp. Combust., 1998: pp. 361–369. doi:10.1016/S0082-0784(98)80424-4.

[5] W. Sun, T. Tao, M. Lailliau, N. Hansen, B. Yang, P. Dagaut, Exploration of the oxidation chemistry of dimethoxymethane: Jet-stirred reactor experiments and kinetic modeling, Combust. Flame. 193 (2018) 491–501. doi:10.1016/j.combustflame.2018.04.008.

[6] Z. Gao, E. Hu, Z. Xu, G. Yin, Z. Huang, Low to intermediate temperature oxidation

studies of dimethoxymethane/n-heptane blends in a jet-stirred reactor, Combust. Flame. 207 (2019) 20–35. doi:10.1016/j.combustflame.2019.05.015.

[7] N. Kurimoto, B. Brumfield, X. Yang, T. Wada, P. Diévart, G. Wysocki, Y. Ju, Quantitative measurements of HO2/H2O2 and intermediate species in low and intermediate temperature oxidation of dimethyl ether, Proc. Combust. Inst. 35 (2015) 457–464. doi:10.1016/j.proci.2014.05.120.

[8] S.L. Fischer, F.L. Dryer, H.J. Curran, Reaction kinetics of dimethyl ether. I: high-temperature pyrolysis and oxidation in flow reactors, Int. J. Chem. Kinet. 32 (2000) 713–740. doi:10.1002/1097-4601(2000)32:12<713::AID-KIN1>3.0.CO;2-9.

[9] H. Guo, W. Sun, F.M. Haas, T. Farouk, F.L. Dryer, Y. Ju, Measurements of H2O2 in low temperature dimethyl ether oxidation, Proc. Combust. Inst. 34 (2013) 573–581. doi:10.1016/j.proci.2012.05.056.

[10] L. Marrodán, F. Monge, Á. Millera, R. Bilbao, M.U. Alzueta, Dimethoxymethane Oxidation in a Flow Reactor, Combust. Sci. Technol. 188 (2016) 719–729. doi:10.1080/00102202.2016.1138826.

[11] L. Marrodán, E. Royo, Á. Millera, R. Bilbao, M.U. Alzueta, High pressure oxidation of dimethoxymethane, Energy and Fuels. 29 (2015) 3507–3517. doi:10.1021/acs.energyfuels.5b00459.

[12] L. Marrodán, Á.J. Arnal, Á. Millera, R. Bilbao, M.U. Alzueta, The inhibiting effect of NO addition on dimethyl ether high-pressure oxidation, Combust. Flame. 197 (2018) 1–10. doi:10.1016/j.combustflame.2018.07.005.

[13] T. Yamamoto, S. Kajimura, Kinetic Study on NO Reduction Using Dimethyl Ether as a Reburning Fuel, Energy and Fuels. 31 (2017) 12500–12507. doi:10.1021/acs.energyfuels.7b02243.

[14] D. Liu, J. Santner, C. Togbé, D. Felsmann, J. Koppmann, A. Lackner, X. Yang, X. Shen, Y. Ju, K. Kohse-Höinghaus, Flame structure and kinetic studies of carbon dioxide-diluted dimethyl ether flames at reduced and elevated pressures, Combust. Flame. 160 (2013) 2654–2668. doi:10.1016/j.combustflame.2013.06.032.

[15] H. Xu, C. Yao, T. Yuan, K. Zhang, H. Guo, Measurements and modeling study of intermediates in ethanol and dimethy ether low-pressure premixed flames using synchrotron photoionization, Combust. Flame. 158 (2011) 1673–1681. doi:10.1016/j.combustflame.2011.01.004.

[16] T. Bolshova, V. Shvartsberg, A. Dmitriev, D. Knyazkov, Flame structure and a compact reaction mechanism for combustion of dimethyl ether at atmospheric pressure, Fuel. 255 (2019) 115752. doi:10.1016/j.fuel.2019.115752.

[17] W. Sun, B. Yang, N. Hansen, K. Moshammer, The influence of dimethoxy methane (DMM)/dimethyl carbonate (DMC) addition on a premixed ethane/oxygen/argon flame, Proc. Combust. Inst. 36 (2017) 449–457. doi:10.1016/J.PROCI.2016.06.145.

[18] U. Pfahl, K. Fieweger, G. Adomeit, Self-ignition of diesel-relevant hydrocarbon-air mixtures under engine conditions, Symp. Combust. 26 (1996) 781–789.

[19] U. Burke, K.P. Somers, P. O'Toole, C.M. Zinner, N. Marquet, G. Bourque, E.L. Petersen, W.K. Metcalfe, Z. Serinyel, H.J. Curran, An ignition delay and kinetic modeling study of methane, dimethyl ether, and their mixtures at high pressures, Combust. Flame. 162 (2015) 315–330. doi:10.1016/j.combustflame.2014.08.014.

[20] F.R. Gillespie, An experimental and modelling study of the combustion of oxygenated hydrocarbons, National University of Ireland, 2014. doi:10.1039/b809078p.